The Loongana (CL) group of carbonaceous chondrites

Journal Pre-proofs

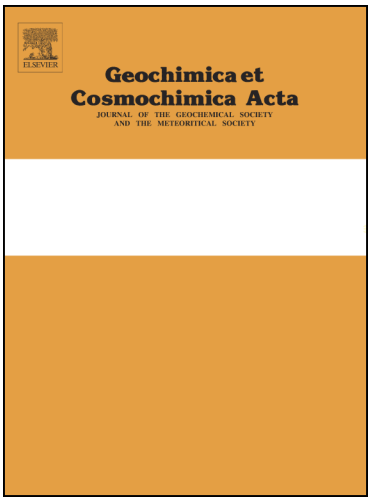

The Loongana (CL) group of carbonaceous chondrites

Knut Metzler, Dominik C. Hezel, Jens Barosch, Elias Wölfer, Jonas M. Schneider, Jan L. Hellmann, Jasper Berndt, Andreas Stracke, Jérôme Gattacceca, Richard C. Greenwood, Ian A. Franchi, Christoph Burkhardt, Thorsten Kleine

PII: S0016-7037(21)00222-2
DOI: https://doi.org/10.1016/j.gca.2021.04.007
Reference: GCA 12153

To appear in: *Geochimica et Cosmochimica Acta*

Received Date: 7 October 2020
Revised Date: 1 April 2021
Accepted Date: 2 April 2021

Please cite this article as: Metzler, K., Hezel, D.C., Barosch, J., Wölfer, E., Schneider, J.M., Hellmann, J.L., Berndt, J., Stracke, A., Gattacceca, J., Greenwood, R.C., Franchi, I.A., Burkhardt, C., Kleine, T., The Loongana (CL) group of carbonaceous chondrites, *Geochimica et Cosmochimica Acta* (2021), doi: https://doi.org/10.1016/j.gca.2021.04.007

The Loongana (CL) group of carbonaceous chondrites

Knut Metzler [a,*], Dominik C. Hezel [b], Jens Barosch [b], Elias Wölfer [a], Jonas M. Schneider [a], Jan L. Hellmann [a], Jasper Berndt [c], Andreas Stracke [c], Jérôme Gattacceca [d], Richard C. Greenwood [e], Ian A. Franchi [e], Christoph Burkhardt [a], Thorsten Kleine [a]

[a] *Institut für Planetologie, University of Münster, Wilhelm-Klemm-Straße 10, 48149 Münster, Germany*
[b] *Institut für Geologie und Mineralogie, University of Cologne, Zülpicher Straße 49a, 50674 Köln, Germany*
[c] *Institut für Mineralogie, University of Münster, Corrensstraße24, 48149 Münster, Germany*
[d] *CNRS, Aix Marseille University, IRD, INRAE, CEREGE, Aix-en-Provence, France*
[e] *Planetary and Space Sciences Research Institute, Open University, Milton Keynes MK7 6AA, UK*

* Corresponding author at: Institut für Planetologie, University of Münster, Wilhelm-Klemm-Str. 10, 48149 Münster, Germany
E-mail address: knut.metzler@uni-muenster.de

Abstract

A coordinated study of the petrology, mineral chemistry, and bulk chemical and isotopic composition of the five ungrouped carbonaceous chondrites Coolidge, Loongana 001, Los Vientos (LoV) 051, Northwest Africa (NWA) 033, and NWA 13400 reveals that these meteorites have a similar set of properties that distinguishes them from the other carbonaceous chondrite groups and allows definition of the new Loongana (CL) group of carbonaceous chondrites. The basic characteristics of the investigated samples are: (1) Lithophile element ratios (e.g., Al/Mg, Si/Mg) are within the typical range of other carbonaceous chondrite groups. (2) Fe-Ni metal abundances are considerably higher than for CV, but similar to CR chondrites. (3) Chondrule size-frequency distributions are similar to CV, but dissimilar to CR chondrites. (4) The mean CAI abundance is ~1.4 vol%, i.e., lower than in CV but much higher than in CR chondrites. (5) Very low amounts of matrix (17-21 vol%), the lowest among the main carbonaceous chondrite groups (CI, CM, CO, CV, CR, CK). (6) Olivine is nearly equilibrated, with mean fayalite (Fa) values between 12.5 mol% (Loongana 001) and 14.7 mol% (NWA 13400) as a metamorphic effect. (7) Lower Al_2O_3 and higher MgO and Cr_2O_3 concentrations in matrix, compared to matrix in CV, CK, and CR chondrites. (8) Volatile elements (Mn, Na, K, Rb, Cs, Zn, Se, Te, Pb, Tl) are considerably depleted compared to all other main carbonaceous chondrite groups, reflecting the low matrix abundance. (9) Bulk O isotope compositions plot along the CCAM line ($\Delta^{17}O$ -3.96 to -5.47‰), partly overlapping with the CV and CK chondrite field but including samples that are more ^{16}O-rich. (10) Unique positions of CL values in the $\epsilon^{54}Cr$-$\epsilon^{50}Ti$ isotope plot, with $\epsilon^{54}Cr$ values similar to CV, CK, and CO, but $\epsilon^{50}Ti$ values similar to CR chondrites. All CL chondrites studied here are of petrologic type 3.9 to 4, indicating that they have been thermally metamorphosed on the parent body. The diagnostic features of CL chondrites detailed here provide a basis for identifying CL members of lower petrologic types. Such samples will be important for determining the pristine state of these meteorites and their components.

1. INTRODUCTION

Chondrites are cosmic sediments, which consist of up to 92% chondrules (e.g. Weisberg et al., 2006; Metzler, 2012), i.e., once molten silicate spherules with sizes mostly between 0.1 and 1 millimeter. Further components are metal and sulfide grains, refractory objects like Ca-Al-rich inclusions and amoeboid olivine aggregates (CAIs, AOAs; e.g. Krot, 2019) and fine-grained matrix. These components occur in variable and often characteristic amounts in the distinct chondrite groups (e.g. Weisberg et al., 2006). Beside the Rumuruti (R) and Kakangari (K) groups, chondrites are subdivided into three classes, namely the ordinary, enstatite, and carbonaceous chondrites. The latter class consists of eight groups, namely the Ivuna-type (CI), Mighei-type (CM), Ornans-type (CO), Vigarano-type (CV), Karoonda-type (CK), Renazzo-type (CR), Bencubbin-type (CB), and CH (high iron) carbonaceous chondrites. Recently, King et al. (2019) defined the Yamato (CY) group of carbonaceous chondrites, which is not well established yet. Of these, the CI group is particularly distinctive, as members of this group do not contain any recognizable chondrules and because their bulk chemistry agrees closely with the heavy element component of the solar photosphere (e.g. Lodders, 2003; Lodders et al., 2009). Each chondrite group is thought to represent a single parent body (or several related parent bodies; e.g., Gattacceca et al., 2020). As such, identification of new chondrite groups is important for understanding the diversity of planetesimals formed in the early solar system, and the processes that led to this diversity.

In addition to the established carbonaceous chondrite groups there are also ungrouped carbonaceous chondrites, which cannot be assigned to one of these groups. Examples are Tagish Lake, Tarda, Essebi and Bells (C2-ungrouped), as well as Ningqiang (C3-ungrouped). Based on similar properties some ungrouped chondrites can be combined into grouplets (consisting of less than 5 individual members), as in the case of Coolidge and Loongana 001 (Kallemeyn and Rubin, 1995). Coolidge is a well-studied meteorite which was originally classified as a CV4 chondrite (Van Schmus, 1969). However, McSween (1977a) concluded that it cannot simply be a metamorphosed sample of a reduced CV chondrite. By contrast, Kallemeyn and Wasson (1982) stated that Coolidge represents a CV chondrite, which “was probably subjected to open-system metamorphic reheating”, a conclusion also reached by Scott and Taylor (1985). However, Kallemeyn (1987) subsequently argued that the strong depletion of volatile elements more likely reflects nebular processes and that this meteorite, therefore, may not be a CV chondrite. Further, Noguchi (1994) found that, compared to the reduced CV chondrite Efremovka, chondrules and matrix in Coolidge are systematically depleted in Na, which also points to a nebular rather than a metamorphic process. Finally, based on petrographic observations and characteristic differences in the inventories of volatile elements, Kallemeyn and Rubin (1995) demonstrated that Coolidge clearly does not belong to the CV group, but together with the newly discovered meteorite Loongana 001, defines a new carbonaceous chondrite grouplet.

During comparative preexamination we found that the three ungrouped carbonaceous chondrites Los Vientos (LoV) 051, Northwest Africa (NWA) 033 and NWA 13400 have similar petrologic, mineralogical and microchemical properties as the Coolidge-Loongana 001 grouplet. The purpose of this study is to verify if these five samples are also similar regarding their bulk chemical and isotopic composition, allowing to group them together into a newly defined group of carbonaceous chondrites.

2. SAMPLES

Five ungrouped carbonaceous chondrite finds, namely Coolidge (USA, found 1937), Loongana 001 (Australia, found 1990), LoV 051 (Chile, found 2010), NWA 033 (Northwest Africa, found 1999), and NWA 13400 (Northwest Africa, found 2016) are investigated in this study. Polished thin sections (PTS), polished epoxy mounts and polished massive samples (slices) of these chondrites were used for petrographic and microchemical characterization. Subsample designations and masses of analyzed material are given in Table 1. To assess data quality and accuracy, representative bulk powder samples of the Allende CV3 chondrite were analyzed together with those of the above specimens. For comparison, we also determined the matrix fraction of Allende ($CV3_{oxA}$), Vigarano ($CV3_{red}$), and NWA 7020 (CR2) as well as the chondrule size-frequency distributions in Allende and NWA 7020.

In the following, the meteorite Loongana 001 is mostly termed Loongana for short and we collectively refer to the five investigated meteorites as “CL chondrites” and “CL samples”. The reasoning for naming the proposed new group “CL” is given in section 5.3.1.

3. METHODS

All subsamples, including those that were subsequently powdered, were investigated and documented by optical and scanning electron microscopy. Samples of each meteorite were powdered in an agate mortar for obtaining the bulk chemical and isotopic compositions by various techniques. Aliquots for all laboratories, with the exception of LA-ICP-MS (Sc, Se, Te), were taken from the same sample powder (Table 1). All chemical data are given in wt.% or ppm (µg/g), respectively.

3.1 Polarizing microscopy

Polished thin sections (PTS) of all samples were used to determine shock stages and weathering grades by polarizing microscopy. Shock stages were determined according to the instructions given in Stöffler et al. (2018); weathering grades have been determined according to Wlotzka (1993). The latter scheme was initially developed to characterize ordinary chondrites, but we adopt it here for the use in cases of metal-rich carbonaceous chondrites.

3.2 Scanning electron microscopy (SEM)

The scanning electron microscope (SEM; Jeol JSM-6610LV) of the Interdisciplinary Centre for Electron Microscopy and Microanalysis (ICEM; University of Münster) was used to characterize the sample textures and to identify mineral phases. All subsamples, including slices for subsequent destructive chemical analysis, were documented by preparing photomosaics (backscatter electron images; BSE) of their polished surfaces. BSE images were also used to identify the various meteorite components (chondrules, CAIs, amoeboid olivine aggregates (AOAs), matrix) and to determine modal

abundances and apparent chondrule sizes. For element mapping we used the SEM (Zeiss Sigma 300 VP) at the Institut für Geologie und Mineralogie, University of Cologne.

3.2.1 Energy-dispersive X-ray (EDX) analysis

Mineral analyses were obtained using an energy-dispersive X-ray (EDX) analyzing system (INCA, Oxford Instruments); all data were automatically normalized to 100 wt.%. Samples and appropriate mineral standards were measured at a working distance of 10 mm and an acceleration voltage of 20 KV. The beam current constancy was controlled by a Faraday cup. The standard ZAF correction procedures were applied (Bence and Albee, 1968). Minerals of known composition (olivine, low-Ca pyroxene and plagioclase from the L6 chondrite Leedey; Feldstein et al., 2001) were measured repeatedly as reference materials to ensure the reproducibility of the EDX system. All mineral analyses were checked for stoichiometry. Since none of the chosen analysis methods in this study was able to measure the bulk chondrite S content of the samples, the following procedure was used to obtain a rough estimate of bulk S concentrations. By using the lowest possible magnification (30x) and a duration of 40 seconds each, EDX analyses of 2-3 different PTS regions of each CL sample and Allende were recorded and averaged. The mean S concentration for Allende, obtained by this method, is 1.67 wt.%, compared to the literature value of 2.10 wt.% (Jarosewich et al., 1987). The obtained values for S concentrations in the other samples were multiplied by the resulting correction factor of 1.26.

3.2.2 Element mapping (phase maps)

We performed element mapping in order to produce phase maps of entire chondrite sections. For this application, the electron beam scanned the stationary sample surface over small areas (~500x400 µm, pixel size ~4 µm) with a dwell time of 10 ms per pixel. The accelerating voltage was set to 20 kV and the aperture diameter to 60 µm. The sample was then moved to a new center and the next map was rastered. The phase maps (Fig. 1; Electronic Annex) were then produced with the PHAPS application (Hezel, 2010). These display every mineral phase in false color and allow their visual identification. We further used the phase maps and the software ”Measure“ (Datinf GmbH, Tübingen, Germany) to determine the modal abundances of CAIs.

3.2.3 Determination of apparent (2D) chondrule sizes

The distributions of apparent (2D) chondrule sizes in the five CL chondrites have been measured, plus those in Allende ($CV3_{oxA}$) and NWA 7020 (CR2) for comparison. For this purpose the software ”Measure“ (Datinf GmbH, Tübingen, Germany) was used, stringently following a raster on the BSE photomosaics to not overlook any chondrule cut face. Apparent chondrule sizes were obtained by measuring the diameters of chondrule cut faces at an angle of 45° from the line of the maximum apparent diameter, and thereby a reasonable average between minimum and maximum is obtained. It was calculated by Eisenhour (1996) that this method provides a good approximation (within 2%) of the diameter of a circle equal in area to that of the measured ellipse. Except for metal grains, sulfide grains, and CAIs, every subrounded, more or less isometric (aspect ratio <~2) object was considered as a chondrule. Chondrules consisting of welded smaller chondrules were measured as one single

chondrule. The same holds for chondrules with adhering layers of smaller chondrules and for the rare chondrules with igneous rims. Chondrule fragments with angular fracture surfaces were only included when their original outline could be unequivocally reconstructed (~half chondrules). Other chondrule fragments and angular monomineralic grains were omitted. It cannot be ruled out that the data sets contain small fractions of unrecognized roundish chondrule fragments, especially in the smallest size bins (<300 µm). Distributions of apparent chondrule sizes (2D) have already measured by this method in several ordinary chondrites (Metzler, 2018; Metzler et al., 2019).

3.3 Electron microprobe (EMPA)

The electron microprobe (JEOL 8900RL) at the Institut für Geologie und Mineralogie (University of Cologne) was used for chemical analysis. Mineral compositions (olivine, low-Ca pyroxene, Ca-rich pyroxene) were determined by spot analyses using a focused, stationary beam of 1 µm, an accelerating voltage of 20 kV, and a beam current of 20 nA. For the analyses of matrix, the beam was defocused to 30 µm and the accelerating voltage was set to 15 kV. The ZAF-algorithm was used for correction (Bence and Albee, 1968). Mineral analyses with totals between 98.5 and 101.5 wt.% were accepted.

3.4 X-ray fluorescence (XRF)

The bulk concentrations of Si, Ti, Al, Cr, Fe, Mn, Mg, Ca, Na, K, P, and Ni have been measured in the five CL samples and an Allende standard powder by X-ray fluorescence techniques. The sample preparation method initially developed by Wolf and Palme (2001) and later modified as described in Stracke et al. (2012) has been used, with a few additional, minor modifications. A sample to standard ratio of 1:30 was used, with typically 120 mg sample material mixed with 3.6 g lithium tetraborate ($Li_2B_4O_7$) flux agent. Before mixing, the sample was pre-treated with aqua regia for a few hours at 120 °C to oxidize the metals. A Claisse LeNeo fluxer was used to automatically produce 27 mm diameter glass disks. The Panalytical Zetium sequential wavelength dispersive X-ray spectrometer at the University of Cologne was used for sample measurements. Standard calibration lines were calculated from 7 identically prepared standard rock samples. The precision for all elements analyzed is below 1% (Wolf and Palme, 2001). An Allende glass disk was produced and measured in the same way as the samples. The obtained data for Allende are in excellent agreement with literature data. Some CL samples showed low totals which most likely resulted from loss of sample material (~2 mg, estimated) during sample preparation as well as loss of material during sample fluxing. The latter was possibly caused by the decomposition of weathering products (hydroxides, calcite) and loss of volatile components (H_2O, CO_2). There was only enough powder to determine the loss on ignition (LOI) of NWA 13400 (2.76%, when 120 mg are heated at 1000°C for 2h). This LOI equals ~3 mg loss of sample material. We recalculated samples with low totals considering an estimated total loss of material of 5 mg. However, some totals are still low, possibly indicating an underestimation of material loss.

3.5 Trace element compositions

Trace element concentrations were analyzed on aliquots of the initial representative meteorite powders and an Allende Standard powder (Allende MS-A). The elements Li, V, Co, Rb, Sr, Y, Zr, Nb, Mo, Cs, Ba, the REE, Hf, Ta, Tl, Pb,Th, and U were analyzed by isotope dilution sector field inductively coupled plasma mass spectrometry (ID-SF-ICP-MS), as described in detail in Stracke et al. (2012).

Concentrations of Sc, Se, and Te in the samples and Allende were analysed by LA-ICP-MS at the University of Münster (Institut für Mineralogie). Sample ablation along linear tracks (50 mm each) across the polished sample surfaces (thin and thick sections) was done using 193 nm ArF excimer laser (Analyte G2, Photon Machines). A repetition rate of 10 Hz and an energy of ~ 3-4 J/cm2 were used throughout the entire session. The beam spot diameter varied between 80 and 100 µm. Elemental analysis has been carried out with an Element 2 mass spectrometer (ThermoFisher). Forward power was 1300 W and reflected power < 2 W, gas flow rates were 1.2 l/m for He (carrier gas of ablated material), 0.8 l/m and 1.1 l/m for the Ar-auxiliary and sample gas, respectively. Cooling gas flow rate was set to 16 l/min. Before starting analysis, the system has been tuned (torch position, lenses, gas flows) on a NIST 612 glass, measuring ^{139}La, ^{232}Th and $^{232}Th^{16}O$ to get stable signals and high sensitivity, as well as low oxide rates ($^{232}Th^{16}O/^{232}Th$ < 0.1%) during ablation. The above elements were quantitatively analysed using the NIST 612 glass as an external standard and ^{43}Ca as internal standard; Ca concentrations had been previously determined by XRF. Concentrations of measured elements were calculated using the Glitter software (Griffin et al., 2008). Standard reference glasses GSD1-G and GSE1-G were analysed as monitor for precision and accuracy. Obtained results match the published range of concentrations given in the GeoReM database (version 24; Jochum et al., 2005).

3.6 Titanium and chromium isotopes

Aliquots (~35 mg each) of the initial representative meteorite powders (equivalent to ~20-30 µg Ti) were digested in HF-HNO_3-$HClO_4$ (2:1:0.05) on a hotplate at 180–200 °C for five days and in aqua regia (HCl-HNO_3) at 130–150 °C for another two days. Thereafter, the samples were dissolved in 12 M HNO_3, and ~65 mg H_3BO_3 was added. Ti was separated from the sample matrix via a two-stage anion exchange chromatography adapted from the previously established procedure from Zhang et al. (2011). In a first step, the sample solutions were loaded onto columns prepacked with 2 ml TOGDA® anion exchange resin, where Ti was eluted in 20 ml 12 M HNO_3–1 wt.% H_2O_2. Afterwards, the Ti cuts were dissolved in 2.5 ml 4 M HF and loaded onto clean-up columns filled with 0.8 ml Bio-Rad® AG1-X8 anion exchange resin, where Ti was eluted in 6 ml 9 M HCl–0.01 M HF.

Titanium isotope measurements were performed in two lines using a ThermoScientific Neptune Plus MC-ICP-MS (Institut für Planetologie, University of Münster) in medium resolving power mode (Zhang et al., 2011). Solutions containing about 200 ppb Ti in 0.3 M HNO_3–0.0014 M HF were introduced through a Cetac Aridus II desolvating system, resulting in a ~3.5×10-10 A ion beam on ^{48}Ti. Measurements consisted of a 30 s baseline measurement (deflected beam) followed by 40 isotope

ratio measurements of 4.2 s each. Mass bias was corrected using the exponential law and $^{49}Ti/^{47}Ti$ = 0.749766. The Ti isotope anomalies are reported as parts per ten thousand deviation (ε-notation) from the terrestrial OL-Ti (Millet and Dauphas, 2014) bracketing standard. The sample uncertainty is reported as the Student-t 95% confidence interval based on repeated analyzes (N=12) of the sample solution.

Chromium was collected during the first step of the two-stage anion exchange chromatography used for the separation of Ti, where Cr is eluted in 25 ml 12 M HNO_3 (+ trace H_3BO_3) together with most other matrix elements. Aliquots (equivalent to ~30 µg Cr) were taken from this solution, dried down, and redissolved in 1 ml 6 M HCl. Afterwards, Cr was separated from the sample matrix using a single-stage anion exchange chemistry for the removal of Fe (Bio-Rad® AG1-X8 anion exchange resin), followed by a two-stage cation exchange chromatography (Bio-Rad® AG50W-X8 cation exchange resin) as described by Yamakawa et al. (2009), including a four-day conversion of $Cr[III]Cl_3/Cr[II]Cl_2$ to Cr^{3+}.

Chromium isotope measurements were performed using a ThermoScientific Triton Plus Thermal Ionization Mass Spectrometer (Institut für Planetologie, University of Münster) in static mode. The sample solutions (containing ~500 ppm Cr in 6 M HCl) were loaded on 4-6 filaments and each filament was measured multiple times, with total ion beam intensities of ~1.4×10-10 A on ^{52}Cr. Instrumental mass fractionation was corrected assuming a constant $^{50}Cr/^{52}Cr$ = 0.051859 and using the exponential law. The data are reported in $\varepsilon^{54}Cr$ values as the parts per ten thousand deviation from the terrestrial NIST SRM3112a Cr standard. The sample uncertainty is reported as the Student-t 95% confidence interval based on repeated analyses (N=8-12).

3.7 Oxygen isotopes

Oxygen isotope analyses were performed at the Open University using an infrared laser-assisted fluorination system (Miller et al., 1999; Greenwood et al., 2017). Samples and standards were weighed out into a Ni sample block with each aliquot having a mass of approximately 2 mg. The block was loaded into a vacuum-tight chamber and heated to 70°C under vacuum overnight to remove surface-bound moisture. The system was then flushed with BrF_5 to reduce the final blank level to <60 nmoles O_2. Oxygen was released from the samples by heating in the presence of BrF_5 using a 50 W infrared CO_2 laser. After fluorination, the released oxygen gas was purified by passing it through two cryogenic nitrogen traps and over a bed of heated KBr to remove any excess fluorine. Oxygen gas was analyzed using a MAT 253 dual inlet mass spectrometer. Overall system precision, as defined by replicate analyses of our internal obsidian standard is: ±0.053‰ for $\delta^{17}O$; ±0.095‰ for $\delta^{18}O$; ±0.018‰ for $\Delta^{17}O$ (2σ) (Starkey et al., 2016).

Oxygen isotopic analyses are reported in standard δ notation, where $\delta^{18}O$ has been calculated as: $\delta^{18}O = [(^{18}O/^{16}O)_{sample}/(^{18}O/^{16}O)_{VSMOW} - 1]\ 1000$ (‰) and similarly for $\delta^{17}O$ using the $^{17}O/^{16}O$ ratio. $\Delta^{17}O$, which represents the deviation from the terrestrial fractionation has been calculated as $\Delta^{17}O = \delta^{17}O - 0.52\ \delta^{18}O$.

3.8 Magnetic measurements

All magnetic measurements were performed at CEREGE (Aix-en-Provence, France). Hysteresis measurements were performed with a Princeton Micromag Vibrating Sample Magnetometer (VSM) with a maximum applied field of 1 T and a sensitivity of ~$5x10^{-9}$ Am^2. The analysis of hysteresis loops provided the ratio of saturation remanent magnetization (M_{RS}) to saturation magnetization (M_S) and the coercive force (B_C). High field susceptibility (χHF) was determined by a linear fit for applied fields > 0.9 T of the hysteresis loops. Remanent coercive force (B_{CR}) was determined by back field experiments performed with the VSM. The low field specific susceptibility (χ in m3/kg) was measured using Agico MFK1 apparatus with sensitivity of $5x10^{-13}$ m3, operating at 200 A/m and a frequency of 976 Hz. We determined the S-300 ratio, defined as the isothermal remanent magnetization (IRM) obtained after applying a 3 T field and then a back field of 0.3 T normalized to the IRM acquired in 3 T. For this experiment, IRM were imparted using a pulse magnetizer from Magnetic Measurement.

4. RESULTS

This study will show that the three ungrouped carbonaceous chondrites Los Vientos (LoV) 051, Northwest Africa (NWA) 033 and NWA 13400 have similar properties as the Coolidge-Loongana 001 grouplet. This makes it possible to combine these five samples into a new carbonaceous chondrite group, which we term the Loongana (CL) group (see section 5.3.1). In the following we define the basic criteria for identifying further members of this group. Since CL chondrites have some similarities to CV_{red} chondrites (e.g., McSween 1977a; Gattacceca et al., 2020) and CR chondrites (e.g., Kallemeyn et al., 1994), our discussion concentrates on these groups when comparing petrographic, chemical and isotopic data of CL chondrites.

4.1 Meteorite textures

The investigated samples are mainly composed of the typical carbonaceous chondrite components, namely Type-I chondrules (FeO-poor, metal rich), refractory inclusions (CAIs, AOAs), inter-chondrule sulfide and metal grains and a fine-grained matrix. Some chondrules of the chemical Type-II occur, as well. Despite the thermal overprint of all investigated CL samples, their Type-I and Type-II chondrules are still discernable by texture and mineral composition (see section 4.7.1.1). Cut faces of the least weathered sample (LoV 051) show well-preserved tiny metal beads within and at the periphery of chondrules. Occasionally, large fragments of chondrules and refractory inclusions occur, but all samples are macroscopically unbrecciated. Their overall textures show some resemblance to the reduced CV chondrites (CV_{red}) and CR chondrites, but differ in having a very low amount of matrix (see section 4.7.3) and consequently a relatively high chondrule abundance. The compositions and textures of Coolidge and Loongana have been described by Noguchi (1994) and Kallemeyn and Rubin (1995). The overall texture of Loongana is shown in Fig. 1 both as a photomosaic of SEM-BSE images (a) and a phase map (b). The following components can be distinguished in Fig. 1: abundant porphyritic (1,6) and rare non-porphyritic chondrules (2), rare Al-rich chondrules (3), chondrule

fragments (4), adhering chondrules (5), olivine chondrules (6) with thick pyroxene rims (7), and CAIs (8). These components are described in detail below (section 4.7).

4.2 Petrologic types

Coolidge and Loongana are listed as being C4-ungrouped in the Meteoritical Bulletin Database (MBDB; www.lpi.usra.edu/meteor/). However, they have also been classified as type 3.8 to 4 and type 3.8 by Kallemeyn and Rubin (1995) and Guimon et al. (1995). The samples NWA 033 and LoV 051 are listed as C3-ungrouped in the MBDB, without allocation to a certain petrologic subtype. NWA 13400 is listed as C3-ungrouped, with a proposed petrologic subtype of 3.9. One of the standard methods to identify a chondrite´s subtype is determining the frequency distribution of fayalite (Fa) values of randomly chosen olivine grains. The percentage mean deviation (PMD) of these values is used as a measure for the equilibration state of a given meteorite (e.g. Hutchison, 2004; his Table 2.6). We determined these distributions in all samples, together with the frequency distributions of ferrosilite (Fs) values of their low-Ca pyroxene grains; the results are shown in Fig. 2. Occasionally, chondrules and chondrule fragments with relict Mg-rich core compositions of olivine can be found in all samples. The PMD values for Coolidge, Loongana, and NWA 033 are below 5% (Table 2), indicating that these samples belong to petrologic type 4, whereas those of LoV 051 and NWA 13400 are between 5% and 10%, indicating a 3.9 subtype.

4.3 Shock stages

All olivine grains in the investigated CL chondrites show undulatory extinction, but grains with planar fractures are rare or absent. Thus, all these samples are weakly shocked (Table 2) and belong to shock stage C-S2 (Stöffler et al., 2018), corresponding to the previously defined shock stage S2 (Stöffler et al., 1991).

4.4 Weathering grades

Most samples are moderately to heavily weathered (W2-W3/4) and crosscut by veins composed of the secondary alteration products of metals and sulfides. Nevertheless, variable amounts of Fe-Ni metal are still visible on cut faces of all samples. The estimated degrees of weathering for the CL samples, which were determined using the scheme of Wlotzka (1993), are given in Table 2. The least weathered CL chondrite of this study is LoV 051 (W1/2), which still contains considerable amounts of pristine metal.

4.5 Magnetic properties

The magnetic properties of all CL chondrites from this study are given in Table 3, together with data for the various CV subgroups (CV_{red}, CV_{oxA}, CV_{oxB}) and CR chondrites for comparison. The magnetic properties of all samples, with the notable exception of LoV 051, have been considerably

modified by terrestrial weathering. Thus, the data for LoV 051 are the most relevant for defining the primary characteristics of the proposed CL group. Its magnetic susceptibility (Table 3) is $\log\chi$ = 5.24 (where χ is in 10^{-9} m^3 kg^{-1}), higher than the corresponding values for the other samples. This difference can be accounted for by terrestrial weathering, which lowers the susceptibility of metal-bearing meteorites (Rochette et al., 2008). The susceptibility of LoV 051 ($\log\chi$ = 5.24) is slightly higher compared to CR chondrites, which have an average $\log\chi$ = 5.04±0.12 as measured on 14 CR meteorites (Rochette et al., 2008), and almost identical to the value for the only CR chondrite fall Renazzo ($\log\chi$ = 5.17). The observed hysteresis loop for LoV 051 is typical of kamacite-bearing rocks (Gattacceca et al., 2014), including a curvature up to above 700 mT, very low coercivity (B_C=3.08 mT), very low M_{RS}/M_S ratio (0.0155), and high B_{CR}/B_C ratio (6.10). Together with the S_{-300} value of 1.00, there is strong evidence that the magnetic mineralogy is dominated by kamacite.

4.6 Modal compositions

The modal compositions of all samples, as well as Allende ($CV3_{oxA}$) and Vigarano (CV_{red}) for comparison, were obtained by point counting on SEM-BSE images. The results for the CL chondrites are summarized in Table. 2. The modal abundances (area% = vol%) of chondrules and chondrule fragments in our samples vary between 67 vol% (Loongana) and 79 vol% (Coolidge). The inter-chondrule metal and sulfide concentration, modified by terrestrial weathering, varies between 3 vol% (Coolidge) and 6 vol% (NWA 033, NWA 13400; Table 2). The concentration of CAIs, measured on phase maps (e.g., Fig. 1), appears highly variable (from 0.1 vol% for Coolidge to 8 vol% for Loongana). For the modal abundance of matrix we obtained values between 17 vol% (LoV 051, NWA 13400) and 21 vol% (NWA 033; Table 2).

To verify our method, we also determined the abundance of matrix in Allende (CV_{oxA}) and Vigarano (CV_{red}) and found values of 46 vol% and 35 vol%, respectively. The value for Allende is in the range of values obtained by McSween (1977a; 38.4 vol%) and Gattacceca et al. (2020; 50 vol%). Our Vigarano value is nearly identical to that of McSween (1977a; 34.5 vol%) and identical to that given in Gattacceca et al. (2020). Thus, our method reproduces literature values well, demonstrating that CL chondrites contain significantly less matrix than CV chondrites and most other carbonaceous chondrites.

4.7 Lithologic components

4.7.1 Chondrules

The investigated CL chondrites consist mainly of chondrules (67-79 vol%; Table 2), including minor amounts of chondrule fragments. In the following the term “chondrules” also includes chondrule fragments, if not stated otherwise.

4.7.1.1 Chondrule textures, types, and mineralogical compositions

Chondrules in the investigated meteorites are mostly porphyritic olivine (PO) and porphyritic olivine-pyroxene (POP) chondrules of Type-I. A high percentage of these show pyroxene rims (see

section 4.7.1.3). Many of these have non-circular, irregular boundaries, which has already been described for Coolidge and Loongana by Kallemeyn and Rubin (1995). Many chondrules in our samples, especially the smaller ones, give the impression of rapidly crystallized droplets from fragmented or shredded melts, which partly accumulated in a viscous state. They show remarkably irregular shapes with lobate outlines and protuberances (Fig. 3a) and sometimes display an amoeboidal shape (Fig. 3b). In some cases it is difficult to define the outlines and boundaries between adjacent objects (Fig. 3c). Many chondrules are the result of adhesive growth from smaller chondrules, i.e., they are part of welded chondrule agglomerates or adhere to the surface of larger chondrules. They form irregular layers of smaller roundish chondrules stacked on top of each other. A striking example is shown in Fig. 3d (white outline), which appears to be an agglomeration of small chondrules and lobate melt droplets around a central chondrule, separated by an Fe-Ni layer (white).

Chondrule olivine is nearly equilibrated in most samples (Table 4; Fig. 2a). The lowest Fa values for olivine grains found in this study (beside the rare relict Mg-rich olivine cores) are around 10 mol%. This value is also the arbitrarily defined boundary between the chondrule Type-I (<10 mol% Fa) and Type-II (McSween, 1977b; Jones et al., 2005; Lauretta et al., 2006). However, the presence of Fe-Ni metal and low-Ca pyroxene with Fs values considerably below 10 mol% in most chondrules in our samples (Figs. 3a-f) relates them to Type-I. In all samples Mg-rich relict olivine cores are found, a further proof that Type-I chondrules were present prior to thermal metamorphism. Occasionally, chondrules of chemical Type-II can be observed in the samples (e.g. BO chondrule in Fig. 3h), identifiable by, e.g., their metal-free composition and the absence of pyroxene rims.

In case of larger chondrules there is a tendency that metal occurs as outer shells (e.g., Fig. 3g). In several cases, metal forms one or two concentric layers within the chondrules (Figs. 3e-f), which may indicate that these structures formed by agglomeratic growth. The largest Fe-Ni metal grains in chondrules were found in LoV 051 (1.1 mm) and Coolidge (1.6 mm). The metal mainly consists of polycrystalline kamacite with small amounts of taenite exsolutions (Fig. 4a). The Ni concentration in kamacite is fairly constant in all samples, with mean concentrations ranging between 7.1 wt.% (NWA 13400) and 8.0 wt.% (NWA 033). Measured Ni concentrations in taenite are variable, with values between 13.5 wt.% and 41.0 wt.%. This is consistent with the results of Scott and Taylor (1985) and Noguchi (1994) who found mean Ni concentrations of 6.4-7.1 wt.% and 19.2-20.9 wt.% for kamacite and taenite, respectively, in Coolidge. In many kamacite grains, tiny subrounded grains of chromite, merrilite, and SiO_2 occur as exsolutions along internal metal grain boundaries (Fig. 4a). A side-by side occurrence of isolated kamacite and taenite grains in chondrules was only rarely observed (Fig. 4b). Polycrystalline, primary sulfide grains (troilite, FeS) up to 500 µm large and frequently intergrown with kamacite, can also be found in these chondrules (Fig. 4c-d). In some chondrule cut faces the sulfide + metal portion exceeds 50 area%. Some metal grains up to 1 mm in size occur outside of chondrules. Chondrule plagioclase compositions are variable (An_{72}-An_{99}) with negligible K concentrations. Noguchi (1994) found values of An_{27}-An_{95} in Coolidge. Plagioclase is concentrated in chondrule mesostases, frequently in the shape of lath-like intergrowths with Ca-rich pyroxene.

Some Al-rich chondrules have been observed in Loongana (Fig. 3g) and LoV 051, and non-porphyritic chondrules (barred olivine; BO) were found in Coolidge and NWA 13400 (Fig. 3h).

4.7.1.2 Chemistry of main minerals

The chemical compositions of the main mineral phases found in chondrules (olivine, low-Ca pyroxene, and Ca-rich pyroxene) were measured by EMPA. Relict Mg-rich olivine cores are occasionally found in all samples, but were not measured during the random analyses. A number of 30 to 49 olivine grains were measured in each sample and the variation of Fa values is shown in Fig. 2a. The broad distributions of LoV 051 and NWA 13400 in this figure mirror the lower grade of metamorphism of these meteorites (petrologic type 3.9; Table 2), compared to the other samples (petrologic type 4; Table2). The distribution widths for LoV 051 and NWA 13400 are similar, but the distribution for the latter appears more asymmetric. This is probably a statistics problem, since 30 olivine grains were analyzed in NWA 13400, compared to 47 grains in LoV 051. The mean Fa values (mol%; Table 4) vary between 12.5 (Loongana) and 14.7 (NWA 13400). The Fa values for Coolidge and Loongana (14.5 and 12.5) are similar to those presented in earlier studies. Scott and Taylor (1985) and Noguchi (1994) found Fa values of 14 in Coolidge; Kallemeyn and Rubin (1995) give a value of 13.6. The mean Fa value for Loongana found by the latter is 11.8. The mean FeO/MnO ratios (wt.%/wt.%) in olivine of our samples vary between 52 (Loongana) and 61 (NWA 13400). Noguchi (1994) found a mean value of 64 in Coolidge, compared to our value of 60.

Between 20 and 49 low-Ca pyroxene grains were measured in each sample and the Fs variation is presented in Fig. 2b. The mean Fs values (mol%; Table 5) vary between 6.6 (NWA 13400) and 10.4 (Loongana). Noguchi (1994) and Kallemeyn and Rubin (1995) found mean Fs values of 10.1 and 9.3, respectively, in Coolidge, compared to our value of 9.4. The mean Fs value of 6.9 for Loongana given in Kallemeyn and Rubin (1995) is somewhat lower than our value (10.4). The mean wollastonite (Wo) values in all samples vary between 0.9 and 1.1 mol% (Table 5). The mean FeO/MnO ratios (wt.%/wt.%) in low-Ca pyroxene are similar and vary between 38 (NWA 13400) and 46 (Coolidge). Low-Ca pyroxene phenocrysts with extremely high Al_2O_3 contents (9-13 wt.%) have been found in a quenched Al-rich chondrule in Loongana (Fig. 3g; dark gray crystals). Similar pyroxene compositions have been found by Noguchi (1994) in a BO chondrule from Coolidge.

Ca-rich pyroxene is another major mineral phase in chondrules. Between 8 and 38 grains were measured in each sample and the mean Fs and Wo variations (mol%) are presented in Table 6. The mean Fs values vary between 4.2 (NWA 13400) and 6.6 (Coolidge) and the mean FeO/MnO ratios (wt.%/wt.%) vary between 13 and 20. The mean Wo values vary between 30.9 (Loongana, NWA 13400) and 38.6 (NWA 033; Table 6).

4.7.1.3 Fractions of chondrules with pyroxene rims

Many of the Type-I PO and POP chondrules, especially the larger ones, are mantled by low-Ca pyroxene layers (Figs. 1, 3e), a typical feature in carbonaceous (and other) chondrites (e.g. Friend et al., 2016; Barosch et al., 2019). We systematically quantified the 2-dimensional fractions of mineralogically zoned chondrules using the produced phase maps. Fractions are lowest in Coolidge (57%), intermediate in LoV 051 (58%), Loongana (59%) and NWA 033 (60%), and highest in NWA 13500 (62%). Barosch et al. (2020) demonstrated that 2D studies underestimate the true (3D) zoned chondrule fractions and proposed a 2D-3D correction factor of 1.24 for carbonaceous chondrites. The

so calculated average 3D zoned chondrule fraction in the investigated samples is ~73%, a value typical of carbonaceous chondrites (Friend et al., 2016; Barosch et al., 2020).

4.7.1.4 Apparent chondrule sizes

We measured the apparent (2D) chondrule sizes in the five CL chondrites as well as in Allende and the CR2 chondrite NWA 7020 for comparison. Obvious chondrule fragments and angular monomineralic grains were excluded from these measurements (see section 3.2.3). The identification of chondrule outlines were sometimes obfuscated by the complex chondrule textures described in section 4.7.1.1). Our chondrule sizes (diameters) include the irregular layers of adhering smaller chondrules and (rarely observed) igneous rims. The statistics for the size-frequency distributions are given in Table 7. The original size data can be found in the Electronic Annex of this publication. We measured between 145 and 512 chondrules per sample and found a fairly restricted range of mean apparent (2D) chondrule sizes, which are between 404 µm (Coolidge) and 477 µm (NWA 13400). These are similar to that of the CV_{ox} chondrite Allende (470 µm), but considerably smaller than that of the CR chondrite (mean 633 µm; Table 7). The same holds for the values of the median sizes and standard deviations. The measured size-frequency distributions of the investigated CL chondrites are shown in Fig. 5a. In Fig. 5b their mean size distribution is compared to the distributions found in the present study for the CV chondrite Allende and the CR chondrite NWA 7020. The mean CL distribution is similar to that of Allende, but the CR distribution differs in having much larger fractions of large (> 600 µm) chondrules and correspondingly lower fractions of smaller chondrules.

4.7.2 Refractory inclusions (CAIs and AOAs)

The largest CAIs found in our study are from NWA 13400 and Loongana, with maximum apparent sizes of 3.8 and 2.8 mm, respectively. The occurrence of CAIs in Loongana and Coolidge has been described by Noguchi (1994) and Kallemeyn and Rubin (1995) with maximum sizes of 500 µm in Coolidge. All CAIs in our samples are fine-grained and consist mainly of an intergrowth of spinel, plagioclase, and Ca-rich pyroxene. Similar CAI textures were also described by Noguchi (1994) for the Coolidge meteorite. A complex CAI in Loongana is shown in Fig. 6a, which consists of fine-grained subunits (anorthite, spinel), rimmed by Ca-rich pyroxene. Some FeS is also present in this CAI. Several other CAIs are rich in FeS, probably a result of secondary alteration on the parent asteroid. An example is shown in Fig. 6b from NWA 13400, which consists of anhedral to euhedral spinel grains, embedded in a fine-grained groundmass of spinel, FeS, and plagioclase. This inclusion is partially rimmed by Ca-rich pyroxene. Spinel grains in all CAIs are zoned, with decreasing Mg- and Al-contents and increasing Cr- and Fe-contents from core to rim. This confirms observations by Noguchi (1994) for Coolidge. In a CAI from this meteorite we found an assemblage of spinel + FeS + TiO_2 (probably rutile; Fig. 6c). This CAI is rimmed by an outer layer of diopside and an inner layer of spinel, possibly remnants of a former Wark-Lovering rim. CAIs in the investigated meteorites are frequently accompanied by large grains of Cl-apatite, either on their edges (up to 500 µm) or in their interiors (up to 100 µm; Fig. 6d). These phosphates possibly formed by the release of Ca during alteration of CAIs. This relation was also observed in Coolidge by Noguchi (1994). Moreover, we found a small (7 µm)

refractory metal nugget with high concentrations of Os, Ir, Pt, and Ru in a CAI in Loongana, placed within a region of altered Fe-Ni metal (Fig. 6e).

Small (< a few hundred μm) amoeboid olivine aggregates (AOAs) were found in Coolidge by Noguchi (1994). We found a large AOA with an apparent maximum size of 900 μm in LoV 051 (Fig. 6f), which consists of a porous part rich in olivine and a more compact part that contains small CAI-like units. These units mainly consist of Ca-rich plagioclase (An_{70}) and chromian spinel.

4.7.3 Matrix

The modal amount of matrix is low in the investigated samples (17-21 vol%; Table 2). The matrix mainly consists of an assortment of olivine grains with smaller amounts of low-Ca pyroxene and some plagioclase. Similar observations were described by Noguchi (1994) for the Coolidge meteorite. Fe-rich materials fills the pore spaces and probably represent oxidation products of metals and sulfides (Fig. 7a), a conclusion also given in McSween (1977a). The grain size distribution of matrix components is bimodal, where larger grains (~2-30 μm) are embedded in a groundmass of smaller grains with sizes mostly between ~0.2 and ~1 μm (Fig. 7b-f). The majority of larger grains represent fragments of formerly larger objects, probably chondrules, with fracture surfaces and irregular outlines. Beside some angular fragments, the smaller grains are a mixture of isometric to slightly elongated grains, which may have crystallized during thermal metamorphism. The mean chemical compositions of matrix in the investigated samples, obtained by EMPA, are listed in Table 8, together with literature data for other carbonaceous chondrite groups. To provide a better comparison with our values, the literature data of McSween and Richardson (1977) in this table have been recalculated to totals of 95%.

4.8 Bulk meteorite elemental compositions

4.8.1 Major and minor elements

The measured bulk concentrations of major and minor elements in the CL chondrites and the Allende reference sample are listed in Table 9, together with literature data for Coolidge, Loongana, and Allende. The measured values for Allende are well within or close to the range of literature values. Our FeO (30.99 wt.%) and Na_2O (0.32 wt.%) values for Coolidge appear high compared to literature values (24.83-27.04 and 0.24-0.26 wt.%, respectively). However, our values for FeO and Na_2O of the Allende reference sample are in the range of literature data, thus showing no systematic analytical bias. None of the chosen analysis methods of this study was able to measure the bulk S content of the samples and we used SEM-EDX data to obtain a rough estimate of the S concentrations (see section 3.2.1). These results are also included in Table 9.

Regarding the concentration ratios of the lithophile elements Si, Mg, and Al, CL data plot within the field of the other carbonaceous chondrite groups (Fig. 8a). Compared to Allende, the CL chondrites are slightly depleted in Al and K and strongly depleted in Mn and Na. Hence, they are chemically well discriminated from CV chondrites and the other groups of carbonaceous chondrites (e.g., Fig. 8b).

4.8.2 Trace elements

The measured bulk concentrations of trace elements in the samples and in the Allende reference sample are listed in Table 10, together with literature data for Coolidge, Loongana, and Allende. Our measurements are plotted in Figs. 8c-d and Figs. 9-10, together with data for major and minor elements. The measured values for Allende are well within or close to the range of literature values (Table 10). One exception is Te, for which we determined a value of 1.21 ppm, compared to literature values between 1.04 ppm (Braukmüller et al., 2018) and 0.94 ppm (Wang et al., 2014). Thus, our Te values for the CL samples may be systematically too high (16%-29%). As noted above, severe weathering effects were detected for Loongana and NWA 033. For example, in these meteorites the light rare earth elements (REE) were enriched during terrestrial weathering, a process described by, e.g., Pourkhorsandi et al. (2017a). These data and some for the other samples are shown in italics in Table 10 and are neither included in the figures nor will they be included in the discussion.

Only few literature data exist on the chemical composition of Coolidge (Kallemeyn and Rubin, 1995; Weckwerth, 2014; Table 10). Compared to these, our values for Sc and Se are higher and those for V and Hf are somewhat lower (Table 10). Compared to literature data (Kallemeyn and Rubin, 1995), our Loongana value for Se is somewhat higher and those for V and Zn are somewhat lower. Again, since our values for the respective elements in the Allende reference sample are in the range of literature data, there appears to be no systematic analytical bias. The investigated CL chondrites are chemically well discernable from the other carbonaceous chondrite groups on Al_2O_3 vs. Zn (Fig. 8c) and Zr vs. Rb (Fig. 8d) plots, which reveal the characteristic depletion of volatile elements such as Rb and Zn.

4.9 Bulk meteorite isotope compositions

4.9.1 Oxygen isotopes

The measured values for $\delta^{17}O$, $\delta^{18}O$, and $\Delta^{17}O$ of the investigated CL chondrites and Allende are listed in Table 11 and plotted in Fig. 11. The compositional fields for CR, CV3, CK, and CO3 chondrites are shown for comparison. All CL samples plot along the Carbonaceous Chondrite Anhydrous Mineral (CCAM) line (Clayton and Mayeda, 1999) with $\Delta^{17}O$ values between -3.96 and -5.47‰. The CL data plot either directly on this line (NWA 033, NWA 13400) or slightly off it and in the direction of the Primitive Chondrule Minerals (PCM) line (Ushikubo et al., 2011). Three of the CL samples (Loongana, NWA 033, NWA 13400) plot within the range of CV3 and CK chondrites, while Coolidge and LoV 051 have considerably lower $^{17}O/^{16}O$ and $^{18}O/^{16}O$ ratios.

4.9.2 Titanium and chromium isotopes

The Ti and Cr isotopic data are provided in Table 12 and visualized in Fig. 12. In Fig. 12a the $\epsilon^{54}Cr$ data are plotted versus the corresponding $\Delta^{17}O$ values and in Fig. 12b the $\epsilon^{54}Cr$ values are plotted versus the $\epsilon^{50}Ti$ data. In such diagrams the dichotomy between non-carbonaceous and carbonaceous chondrites is strikingly evident (Warren, 2011; Kleine et al., 2020). Although the $\epsilon^{54}Cr$ values of the five CL chondrites are similar to the mean compositions of CO and CV chondrites (Fig. 12a), the CL chondrites plot in a distinctly different region of the $\epsilon^{54}Cr$-$\epsilon^{50}Ti$ diagram, where they do not overlap with the compositions of CO and CV chondrites (Fig. 12b). Instead, in terms of $\epsilon^{50}Ti$ the CL chondrites are

more similar to CM and CR chondrites. All CL chondrites have indistinguishable ε^{50}Ti and ε^{54}Cr values, and so the mean Ti and Cr isotope composition of the CL group (Table 12) can be precisely defined from these data. This in turn makes it possible to use these data for evaluating the genetic relationship of CL chondrites relative to other carbonaceous chondrite groups.

5. DISCUSSION

5.1 Characteristics of CL chondrites and differences to other chondrite groups

The investigated samples share many textural, chemical, and isotopic properties. Macroscopically they remotely resemble CV_{red} and CR chondrites, but there are many differences to these and other carbonaceous chondrite groups, as discussed in the following.

5.1.1 Chondrules

Most chondrules are PO and POP varieties of Type-I, rich in Fe-Ni metal. Many small chondrules show a remarkably irregular outer shape with lobate outlines and protuberances (Fig. 3a) or even have an amoeboidal shape (Figs. 3b,c). Many of the small chondrules are concentrated in layers around larger chondrules (Fig. 3d). However, such textures are not unique to these samples, but were occasionally observed by us in the CV_{red} chondrite Vigarano and the CR chondrite NWA 7020, as well. Lobate chondrules also exist in CO chondrites and are explained as having formed from reheated chondrule fragments, i.e., by rounding of fracture surfaces by minor melting (Rubin and Wasson, 2005). Based on the refractory element diversity of different lobes in a given chondrule, Jacquet (2021) concluded that lobate chondrules formed by the collision of preexisting droplets. A formation of lobate chondrules in CL chondrites by droplet collision would fit well to the observed chondrule textures (e.g., Fig. 3d). A distinctive feature of the CL samples is their high chondrule abundance (67 to 79 vol%; Table 2). Kallemeyn and Rubin (1995) found nearly the same chondrule abundance in Loongana (~70% vs. 67% in this study), but a lower abundance in Coolidge (60-65% vs. 79% in this study), possibly reflecting sample heterogeneity. McSween et al. (1977a) found 67 vol% chondrules in Coolidge. For comparison, chondrule concentrations in CV and CR chondrites are 45% and 50-60%, respectively (Krot et al, 2014), i.e., considerably lower than in CL chondrites.

5.1.2 Apparent chondrule sizes

The observed range of mean apparent chondrule sizes in the CL samples is restricted to values between 404 and 477 µm (Table 7). To verify our method, we also measured the apparent (2D) chondrule sizes in the CR2 chondrite NWA 7020 and the CV_{OxA} chondrite Allende (Table 7; Fig. 5b). It is found that the values of mean chondrule sizes in CLs overlap with those in the CV chondrite Allende (470 µm; Table 7). Other statistical parameters of the CL chondrites size-frequency distributions (median size, standard deviation, and skewness) are also similar to those displayed by Allende (Table 7), hinting at a remote relationship to CV chondrites. The CL mean sizes are distinctly smaller than that of the CR chondrite NWA 7020, which shows a mean size of 633 µm and a much more symmetric distribution (skewness of only 1.20, compared to 1.69-2.60 in CLs; Tab. 7).

Literature values of mean apparent chondrule sizes for Coolidge and Loongana (610 µm and 700 µm; Kallemeyn and Rubin, 1995) are larger than those found by us (404 µm and 414 µm). The likely explanation is that we measured a large number of chondrules (145 and 235; Table 7) on BSE photomosaics, whereas the literature values were obtained from only 23-52 chondrules (Kallemeyn and Rubin 1995) using optical microscopy. This could have led to an overrepresentation of large chondrules in their statistics.

Our mean value for the CR2 chondrite (633 µm) is in the range of published values for five other CR chondrites (490-770 µm) and close to the corresponding average value (658 µm; Kallemeyn et al., 1994). In case of Allende a verification of our mean value (470 µm) is more complicated since literature data vary considerably, with mean values of 915 µm (Teitler et al., 2010), 765 µm (Gattacceca et al., 2020), and 310 µm (Simon et al., 2018). Sample inhomogeneity may be partly responsible for these variations. Furthermore, the different methods of investigation certainly contribute to these differences, i.e., chondrule separation (true chondrule sizes; Teitler et al., 2010), optical microscopy (apparent chondrule sizes; Gattacceca et al., 2020), and scanning electron microscopy (apparent chondrule sizes; x-ray compositional images, Simon et al., 2018; BSE images, this work). Furthermore, the classification of small subrounded particle cut faces as chondrules or fragments is a source of subjective bias.

From the presented results it can be concluded that the chondrule-size-frequency distributions and mean chondrule sizes in CL chondrites are similar to each other and to those in CV chondrites, but dissimilar to those in CR chondrites (Fig. 5; Table 7).

5.1.3 Mean olivine compositions

Similar mean compositions of olivine (Fa 12.5-14.7 mol%; Table 4) are a further distinctive feature of CL chondrites. However, this property is of secondary origin, established by thermal metamorphism on the parent body. This cannot not be a criterion for recognizing unequilibrated CL samples that may be identified in the future (see section 5.3.3). On the other hand, this characteristic range of mean Fa values discerns the CL samples from metamorphosed CV and CR meteorites, since mean Fa values in the latter are much higher. For example, olivine in the CV4 chondrite NWA 8418 (Mallozzi et al., 2018), originally classified as C3 (MBDB), shows a mean Fa value of~40 mol%, with a pronounced peak at ~38 mol%, far away from the Fa values in CL samples. The CR6 chondrites NWA 6921, NWA 7317, and NWA 11561 show mean Fa values between 29 and 38 mol% (MBDB), which is also much higher than in CL chondrites. Due to these differences it is obvious that CL chondrites do not represent thermally altered CV and CR chondrites.

5.1.4 Fe-Ni metal abundance

Another distinctive feature of CL compared to CV chondrites is the high amount of Fe-Ni metal, which influences their magnetic properties. The magnetic susceptibility of LoV 051, the least weathered sample, is $\log\chi = 5.24$ (where χ is in 10^{-9} $m^3.kg^{-1}$), which is similar to the mean value for CR chondrites of $\log\chi = 5.04\pm0.12$ (Table 3; Rochette et al., 2008). The value for the saturation magnetization M_S (32.3 Am^2/kg) translates into a kamacite content of 14.4 wt.% for LoV 051. The hysteresis properties of the investigated samples are similar to those of Renazzo CR chondrite. They

697 are markedly different from those of CV chondrites (Weisberg et al., 1997), including CV_{red} that show
698 the highest Fe-Ni metal abundances. Indeed, CV_{red} meteorites contain much less metal than LoV 051,
699 i.e., 2.73±1.12 vol% (average ± s.d., n=9; Bonal et al., 2020), translating into 6.8±2.8 wt.%.
700
701 *5.1.5 CAI abundances*
702 The CAI abundances appear to be another characteristic property of the CL chondrites, although
703 our data base is limited. The modal abundance of CAIs is highly variable (from 0.1 vol% for Coolidge
704 to 8 vol% for Loongana; Table 2), probably due to the small section sizes (52 - 361 mm^2; Table 1). It
705 was shown by Hezel et al. (2008) that section sizes <1000 mm^2 do not give representative results, as
706 CAI abundances follow a Poisson distribution in thin sections. A clear hint on this is the observation
707 that the sample with the apparently highest CAI abundance (Loongana) shows the lowest bulk Al_2O_3
708 concentration (Table 9). Taking all measurements together (655 mm^2), the average CAI abundance is
709 1.4 vol%. Hence, our best guess for the CAI concentration in these samples is ~1.4 vol%, which is
710 much higher than in CR chondrites (0.12 vol%) and distinctly lower than in CV chondrites (~3 vol% or
711 ~4 vol%; Hezel et al., 2008; Ebel et al, 2016). Our estimate is comparable to that given in Kallemeyn
712 and Rubin (1995) for Coolidge and Loongana (1-2 vol%).
713
714 *5.1.6 Matrix*
715 Complementary to the high chondrule concentration, the low amount of matrix (17-21%; Table 2) is
716 another important distinctive feature of CL chondrites. The mean modal abundances of matrix in CV
717 and CR chondrites are much higher, i.e., 52 vol% and 40 vol% in CV_{ox} and CV_{red}, respectively,
718 (Gattacceca et al., 2020) and 35 vol% in CR chondrites (Schrader et al., 2011). Our value of 18% for
719 Coolidge is nearly identical to the value (17.6%) given by McSween (1977a). The value for matrix in
720 Coolidge as obtained by Kallemeyn and Rubin (1995) is higher (~30%), but may reflect sample
721 inhomogeneity. Their value for matrix abundance in Loongana is ~20%, identical to the value found in
722 the present study (Table 2).
723 It was found by Noguchi (1994) that Coolidge matrix is depleted in Na, compared to the reduced
724 CV chondrite Efremovka. This can be confirmed by our measurements, since we found a Na_2O
725 concentration of 0.25 wt.% in Coolidge matrix, which is only half the concentration found in Vigarano
726 Matrix (0.54 wt.%; McSween and Richardson, 1977; Table 8). However, the Na_2O concentration in CL
727 matrix varies considerably between 0.09 wt.% (NWA 13400) and 0.53 wt.% (NWA 033), with a mean
728 value of 0.30 wt.% (Table 8). The mean concentration of Al_2O_3 in CL chondrite matrix (1.84 wt.%) is
729 considerably lower than in the matrices of CV, CR and CK chondrites (2.48-7.63 wt.%; Table 8).
730 Another striking difference is the enrichment of Cr_2O_3 (mean value 0.71 wt.%) in the CL chondrite
731 matrix, compared to 0.40-0.44 wt.% in CV, CK, and CR chondrites (Table 8). This characteristic was
732 already mentioned by McSween and Richardson (1977) for the Coolidge chondrite. The clearest
733 difference to matrix compositions of CV, CR, and CK chondrites are the extraordinarily high MgO
734 concentrations in the CL matrices (mean 28.3 wt.%), compared to mean values of 18.4-21.7 wt.% in
735 the other groups (Table 8). Since olivine and pyroxene are the main carriers of Mg, we have to
736 conclude that these minerals occur in higher abundances in CL matrix than in CV, CK, and CR matrix.
737 This may be a primary characteristic of CL matrix or be the result of matrix modification during thermal

metamorphism. The bimodal size distribution of matrix silicates (see Fig. 7) may indicate the growth of small secondary olivine and pyroxene, by which an enrichment of Mg in bulk matrix may be partly explained. Furthermore, S is considerably depleted in the CL matrix (mean value 0.14 wt.%), compared to CR chondrites and the CV subgroups. Only CK chondrites show a lower mean concentration (0.09 wt.%). However, CL3.9/CL4 and CK4 chondrites were affected by thermal metamorphism on their parent asteroids, by which their fine-grained matrix may have undergone considerable chemical modifications.

5.1.7 Bulk chemical compositions

The bulk chemical compositions of the five investigated CLsamples prove that they belong to the class of carbonaceous chondrites. This is shown in Fig. 8a, where the mean bulk Si/Mg versus Al/Mg element ratios of the CL group are plotted (red filled circle). The CL data plot among the mean data for the other major carbonaceous chondrite groups (Hutchison, 2004; his table 2.1), close to the value for the CK group. Ordinary and R chondrites plot close to each other, but in a distinctly different field in the diagram. The mean values for both enstatite chondrite groups (EH and EL) are also located far away from the field for carbonaceous chondrites. The most characteristic chemical difference between CL chondrites and all other carbonaceous chondrite groups (besides CB and CH) is their strong depletion of volatile lithophile and chalcophile elements. The differences to the CV chondrite Allende can be seen in Tables 9-10 and Figs. 9-10. This distinctive feature was previously noticed for Coolidge and Loongana (e.g. Kallemeyn and Wasson, 1982; Kallemeyn and Rubin, 1995; Weckwerth, 2014). The CL chondrites are well resolved from other carbonaceous chondrite groups on, for example Al_2O_3 vs. MnO (Fig. 8b), Al_2O_3 vs. Zn (Fig. 8c), and Zr vs. Rb (Fig. 8d) plots, since volatile elements like Mn, Zn, and Rb are moderately to strongly depleted.

In Fig. 9a the CI-normalized concentrations (Lodders et al., 2009) of all measured lithophile elements in the CL samples and the Allende reference sample are shown (see Table 10), together with Allende literature data (dotted line). Elements in Figs. 9 and 10 are arranged in the order of increasing volatility (Wood et al., 2019). While elements from Zr (most refractory) to ~Eu in the CL chondrites and Allende exhibit similar CI-normalized abundances, elements from V to Cs are increasingly depleted. This trend steepens for elements more volatile than Cr (Mn, Na, K, Rb, and Cs), with much stronger depletions in the CLs compared to Allende. This can also be seen in the mean CL values in Fig. 9b, when compared to mean values for the other carbonaceous chondrite groups (CM, CO, CV, CR, CK4). The CL chondrites are characterized by strong enrichments of refractory and the strongest depletions of volatile elements among all carbonaceous chondrite groups.

Figure 10 shows the CI-normalized concentrations of siderophile and chalcophile elements in CL chondrites. In Fig. 10a the values for individual CL chondrites are given, again in comparison to Allende values (measurements and literature data). In Fig. 10b the mean CL values are given, compared to the mean values of the other main carbonaceous chondrite groups. For the siderophile elements Mo, Ni, Co, Fe, and P all samples show a similar pattern, which is also similar to that of the Allende chondrite (Fig. 10a). The mean CL values (Fig. 10b) are in the range of those in the other groups, with the highest concentration of Mo, the most refractory element in this plot. The chalcophile element concentrations in the CL chondrites show some scatter, but are consistently lower than in

Allende (Fig. 10a). The mean CL values for chalcophile elements are plotted in Fig. 10b, compared to mean values for the other carbonaceous chondrite groups. The CL mean values indicate the strongest depletions of these elements compared to all other groups, which is in line with the strong depletions of volatile lithophile elements (Fig. 9). Recently, Braukmüller et al. (2018) have shown that concentrations of volatile elements with 50% condensation temperatures below 800 K (from Zn to Tl in Fig. 10) systematically differ between the various groups, but are depleted to about the same extent in a given group (Fig. 10b). Therefore, they termed them "plateau volatile elements". The CL chondrites investigated in this study deviate somewhat from a plateau-like pattern, since the Zn, Pb, and Tl concentrations appear low compared to the Se and Te concentrations (Fig. 10b). However, Braukmüller et al. (2018) also showed that in the ungrouped carbonaceous chondrite EET 96026 the relative concentrations of the plateau volatile elements were strongly modified during thermal metamorphism. As such, the deviations for the CL chondrites observed in this study may also reflect some element fractionations during thermal metamorphism. This issue will be further discussed below (section 5.2).

5.1.8 Bulk isotopic compositions

Figure 11 shows that the O isotopic compositions of CL chondrites (Table 11) do not define a tight cluster, but exhibit a range of isotopic compositions along the CCAM line ($\Delta^{17}O$ -3.96 to -5.47‰). This is also typical of the CV and CK groups and may be indicative of some form of relationship between these groups. Two samples (Coolidge, LoV 051) fall outside the compositional fields of CV and CK chondrites and have considerably lower $^{17}O/^{16}O$ and $^{18}O/^{16}O$ ratios. However, Gattacceca et al. (2020) presented O isotope data of two Antarctic CV_{red} chondrites, which overlap with our values for Coolidge. On the other hand, the O isotopic compositions of CL chondrites are clearly distinct from CR chondrites, ruling out any genetic link between these two chondrite groups.

The investigated CL samples have a mean $\varepsilon^{54}Cr$ value of 0.71 ± 0.06 (Table 12) , which is slightly lower than the $\varepsilon^{54}Cr$ value of CV chondrites (mean $\varepsilon^{54}Cr$ = 0.87 ± 0.07; Burkhardt et al., 2019) and can clearly be distinguished from the mean $\varepsilon^{54}Cr$ values of CM and CR chondrites (Fig. 12; Trinquier et al., 2007; Qin et al., 2010). The only known carbonaceous chondrite group with similar $\varepsilon^{54}Cr$ are the CO chondrites. By contrast, all CL samples exhibit significantly lower $\varepsilon^{50}Ti$ values than typically observed for CV, CO, and CK groups (e.g. Trinquier et al., 2009; Zhang et al., 2012; Burkhardt et al., 2019), and their weighted mean $\varepsilon^{50}Ti$ of 2.60 ± 0.05 (Table 12) is also significantly lower than the $\varepsilon^{50}Ti$ of 3.21 ± 0.11 measured for bulk Allende (CV3) in the present study. As such, the Ti isotopic composition of CL chondrites is more similar to that of CM and CR chondrites (Fig. 12b). Thus, on a plot of $\varepsilon^{50}Ti$ vs $\varepsilon^{54}Cr$ the CL chondrites define a distinct cluster with a unique position, making this plot particularly useful as a means of demonstrating that the CL chondrites are isotopically distinct from the other carbonaceous chondrite groups.

CAIs are highly enriched in Ti and are characterized by large $\varepsilon^{50}Ti$ excesses (e.g., $\varepsilon^{50}Ti \approx 9$; Davis et al., 2018; Render et al., 2019), and, as such, exert a strong control on the Ti concentration and Ti isotopic composition of bulk carbonaceous chondrites (e.g., Burkhardt et al., 2019). For instance, CAI-free CI chondrites display the lowest Ti concentrations and $\varepsilon^{50}Ti$ excesses among the carbonaceous chondrites, whereas the CAI-rich CV, CO, and CK chondrites have the highest Ti concentrations and

exhibit large ε^{50}Ti excesses (e.g. Trinquier et al., 2009). As such, the less-pronounced ε^{50}Ti excesses of the CL relative to CV, CO, and CK chondrites suggest that CL chondrites are characterized by significantly lower CAI abundances compared to the other groups of carbonaceous chondrites. Note that given the large amount of sample material used for analyses, it is very unlikely that the less-pronounced ε^{50}Ti excesses of the CL chondrites of this study reflect a sampling bias, that is, an unrepresentative lower CAI abundance in the selected sample aliquot. Instead, the lower ε^{50}Ti of CL compared to CV chondrites is fully in line with petrographic observations indicating that CL chondrites contain only about 1.4 vol% of CAIs (see sections 4.7.2 and 5.1.5), in contrast to ~3 vol% in CV chondrites (Hezel et al., 2008). Surprisingly though, CL chondrites have essentially the same Ti content as the CAI-rich CV chondrites, indicating that CL chondrites incorporated a Ti-rich component which, unlike CAIs, is not characterized by large ε^{50}Ti excesses. The origin and nature of this component is difficult to assess, but we note that Na-Al-rich chondrules from ordinary chondrites contain a refractory component which is chemically CAI-like, yet is characterized by ε^{50}Ti deficits and not excesses (Ebert et al., 2018). Incorporation of such material into CL chondrites may, therefore, account for their elevated Ti content but lack of more pronounced ε^{50}Ti excesses.

Contrary to Ti, CAIs are depleted in Cr relative to the major chondrite components (e.g., chondrules and matrix), and so varying CAI abundances have a negligible effect on the Cr isotopic composition of bulk chondrites. Instead, the ε^{54}Cr variations among carbonaceous chondrites predominantly reflect variable amounts of chondrules and matrix. For instance, Hellmann et al. (2020) have shown that among the major carbonaceous chondrite groups (except CR) ε^{54}Cr is correlated with the mass fraction of matrix in each group (Fig. 13a). These authors have also shown that bulk carbonaceous chondrites plot along a mixing line between the mean composition of CV, CO, and CM chondrules and bulk CI chondrites, indicating that the ε^{54}Cr variability reflects different mixtures of ^{54}Cr-rich and CI-like matrix and ^{54}Cr-poorer chondrules. The CR chondrites plot off this mixing line, because their chondrules have a distinct ε^{54}Cr composition, either because they formed from different precursor material and/or because they formed later (Hellmann et al., 2020). Assessing whether the CL chondrites plot on the chondrule-matrix mixing line defined by the other carbonaceous chondrite groups requires conversion of their matrix volume fraction (~19 vol% on average; Table 2) to matrix mass fraction. Following the approach of Hellmann et al. (2020) this results in an average matrix fraction of 12 wt.% for the CL chondrites. Using this value together with the mean ε^{54}Cr of ~0.7 reveals that CL chondrites plot exactly on the mixing line between mean CV, CO, and CM chondrules and bulk CI chondrites (Fig. 13a). On the one hand this indicates that the ε^{54}Cr values of CL chondrules are similar to those of the CV, CO, and CM chondrules and on the other hand that the low ε^{54}Cr values of bulk CL chondrites reflects their low matrix fraction.

5.2 Volatile depletions: nebular fractionation or thermal metamorphism on the parent body?

The bulk concentrations of volatile elements systematically co-vary among the distinct carbonaceous chondrite groups (CI, CM, CV, CO, CR) and, like the bulk ε^{54}Cr values, are positively correlated with the group-specific matrix abundances (Hellmann et al., 2020). This is illustrated in Figs. 13b-d, where the matrix mass fractions of the carbonaceous chondrite groups are plotted against their

average concentrations of the volatile elements Zn, Se, and Te. The CL group, together with the other carbonaceous chondrite groups, plot on these correlation lines, corroborating earlier conclusions that the variable volatile depletions among the carbonaceous chondrites predominantly reflect variable matrix abundances (e.g., Alexander, 2019; Hellmann et al., 2020). A corollary of this observation is that the strong volatile depletion of CL chondrites reflects their very low matrix abundance.

Since the investigated CL chondrites were heated on their parent asteroid, we also have to consider the possibility of volatile loss by this process. Such effects were investigated for Allende (CV_{oxA}; Wulf et al., 1995) and for Murchison (CM2; Braukmüller et al., 2018) with heating experiments under oxidizing and reducing conditions. The depletion of the volatile lithophile elements Mn, Na, K, Rb, and Cs is one of the most distinctive features of CL chondrites (Figs. 8, 9). However, Braukmüller et al (2018) did not observe considerable depletions of these elements during their heating experiments (Mn was not considered). The behavior of Mn was investigated by Wulf et al (1995) who found that Mn does not show any depletions, even not in the experiments performed at 1300°C, neither under oxidizing nor reducing conditions. Considerable depletions of chalcophile elements like Zn, Te, Pb, and Tl were found by Wulf et al. (1995) and Braukmüller et al. (2018) under reducing conditions. However, the experimentally produced depletion of Pb is higher than for Zn (Braukmüller et al., 2018), whereas these two elements are depleted in CL chondrites by about the same magnitude (Fig. 10). From these observations we conclude that the consistently low bulk concentrations of volatile lithophile elements (Mn, Na, K, Rb, and Cs) and volatile chalcophile elements (Zn, Se, Te, Pb and Tl) in CL chondrites are a primary feature and do not result from thermal metamorphism on the parent body. However, it is possible that the latter process affected the chalcophile element concentrations in the CL samples to some extent. In particular, the relative abundances of the plateau volatile elements (Zn, Se, Te, Pb, Tl; Braukmüller et al., 2018) appear to have been modified by this process, because the ratios of these elements vary considerably among individual CL samples (Fig. 10a), possibly indicating local redistribution on the parent body.

5.3 Proposal for the new Loongana (CL) group of carbonaceous chondrites

Based on their common characteristics we conclude that the five investigated meteorites can be combined together to form a new group of carbonaceous chondrites. The foundation for this was given by Kallemeyn and Rubin (1995), who defined the Coolidge-Loongana grouplet.

5.3.1 Proposed naming as the CL group of carbonaceous chondrites

Among the investigated samples only Coolidge was given an individual meteorite name; the others are named by serial numbers (Table 1). Hence, the first alphabetic character of Coolidge would be the best candidate to name this group, leading to the CC group of carbonaceous chondrites, which is precluded by the already existing CC meteorite class (CC for carbonaceous chondrites). Since Loongana 001 was the first meteorite for which a close relation to Coolidge was described (Kallemeyn and Rubin, 1995), we propose to use its first alphabetic character for naming this new group as the CL group.

5.3.2 Other meteorites previously proposed to belong to the Coolidge-Loongana grouplet

There are some other ungrouped carbonaceous chondrites, which may belong to the Coolidge-Loongana grouplet. However, as will be argued below, none of these samples share the characteristic properties of the five CL chondrites of this study. Nevertheless, future determination of Ti and Cr isotopic compositions of these meteorites will probably help to clarify their relationship to the CL chondrites and other groups of carbonaceous chondrites.

5.3.2.1 NWA 779

Weckwerth et al. (2001) proposed that NWA 779 belongs to the Coolidge-Loongana grouplet. However, the determined mean Fa concentration in olivine is 21 mol%, very different from the Fa values of Loongana (12.5 mol%), Coolidge (14.5 mol%) and the other samples described by us (12.8-14.7 mol%; Table 4). Moreover, several volatile element concentrations are considerably higher in NWA 779. These are, for example K_2O (0.08 wt.% in NWA 779 compared to 0.01-0.02 wt.% in the CLs; Table 9), MnO (0.20 wt.% compared to 0.14-0.16 wt.%; Table 9), and Zn (110 ppm compared to 33-57 ppm; Table 10). A further obvious difference is the low concentration of Ni and Co in NWA 779 (6000 and 300 ppm, respectively), compared to 12800-13900 ppm and 560-600 ppm, respectively, in the five investigated CL meteorites (Table 9). This is difficult to explain by terrestrial weathering, since most of the CL samples are also strongly weathered. Obviously, NWA 779 contains (as a primary feature) much lower amounts of Fe-Ni metal than the CL meteorites. For these reasons, NWA 779 does not belong to the proposed CL group, but appears to be correctly classified as CV3 (of high petrologic type) in the MBDB.

5.3.2.2 Hammada al Hamra (HaH) 073

Weckwerth and Weber (1998) and Weckwerth (2014) conclude that Hammada al Hamra (HaH) 073, currently classified as C4 (MBDB), belongs to the Coolidge-Loongana grouplet. The O isotopic composition of this sample plots within the range of CV-CK chondrites on the CCAM line in $\delta^{18}O$-$\delta^{17}O$ space (MBDB). Its mean Fa content in olivine is 17.9 mol%, i.e., outside the range of the five investigated CL samples (12.5-14.7 mol%) and it contains considerably more (~33 vol%) fine-grained matrix (Weckwerth and Weber, 1998) than the here studies samples (17-21 vol%; Table 2). The mean apparent chondrule size of HaH 073 is 580 µm (Weckwerth and Weber, 1998), also outside the range of the measured CL values (404-477 µm; Table 7). The concentrations of Ni and Co in HaH 073 (12600 and 575 ppm, respectively; Choe et al., 2010) are slightly lower than those in the CL samples (12800-13900 ppm and 560-600 ppm, respectively; Table 9), indicating a slightly lower abundance of Fe-Ni metal. The concentrations of many volatile elements in HaH 073 are considerably higher than in CL chondrites. The Na_2O concentrations in the latter are 0.18-0.32 wt.% (Table 9), compared to 0.51 (Weckwerth and Weber, 1998) and 0.50 (Choe et al., 2010), respectively, in HaH 073. The same is true for K, which shows low concentrations of 0.01-0.02 wt.% in CL chondrites (Table 9) and high concentrations between 0.034 (Choe et al., 2010) and 0.040 wt.% (Weckwerth and Weber, 1998) in HaH 073. The MnO concentration in HaH 073 (0.17 wt.%; Weckwerth and Weber, 1998; Choe et al., 2010) is somewhat higher than in the CL samples (0.14-0.16 wt.%), and the Zn concentration is distinctly higher, namely 63-66 ppm (Weckwerth and Weber, 1998; Choe et al., 2010), compared to

33-57 ppm in our samples. However, Weckwerth (2014) revised several HaH 073 values from an earlier publication (Weckwerth and Weber, 1998) and some of the new results are closer to the range of CL values, e.g., MnO (0.13 wt.%) and Zn (20 ppm). However, the new data for Na_2O (0.43 wt.%) and K_2O (0.037 wt.%) are still much higher than those in the CL chondrites. Taking the above differences together, it appears that HaH 073 may be related to, but is not a member of the CL chondrite group.

5.3.2.3 Sahara 00182

Weckwerth (2014) argued that Sahara 00182 (C3-ung; MBDB) belongs to the Coolidge-Loongana grouplet. This meteorite with a mean Fa value of 7.8 mol% (Smith et al., 2004) is probably paired with Sahara 00177 (C3/4-ung; MBDB), which shows a mean Fa value of 7.6 mol%. These Fa values are far outside the range for CL chondrites (12.5-14.7 mol%). Due to the absence of phyllosilicates, Weisberg (2001) classified Sahara 00182 as the first CR3 chondrite. However, its oxygen isotopic composition plots on the CCAM line in $\delta^{18}O$-$\delta^{17}O$ space (MBDB), which excludes a relationship to CR chondrites. A mean apparent chondrule size of 1010 µm was determined by Smith et al (2004), a much higher value compared to the CL samples (404-474 µm; Table 7). The modal abundance of matrix is ~28 vol% (Smith et al., 2004), a value which is outside the observed range in CL chondrites (17-21 vol%; Table 2). The concentration of Ni and Co in Sahara 00182 (14900 and 691 ppm, respectively; Choe et al., 2010) are higher than CL values (12800-13900 ppm and 560-600 ppm, respectively; Table 9), indicating a higher abundance of Fe-Ni metal. Furthermore, Na_2O and K_2O concentrations in Sahara 00182 are higher than in the CL chondrites, namely 0.29-0.36 and 0.03 wt.%, respectively (Choe et al., 2010; Weckwerth, 2014), compared to 0.18-0.27 wt.% and 0.01-0.02 wt.% (Table 9). Due to these differences it is improbable that Sahara 00182 is closely related to the CL chondrites. The strongest argument against such a relationship is provided by the distinctly different chemical composition of matrix. The SiO_2 and MgO concentrations in the matrix of Sahara 00182 are 24.2 and 21.7 wt.%, respectively, compared to 30.3 and 28.3 wt.% in the CL chondrites (Table 8). These values from Smith et al. (2004) have been recalculated to totals of 95 wt.% for comparison. There are even more extreme differences in the matrix concentrations of CaO and S. While the matrix in CL chondrites is characterized by very low concentrations of CaO and S (0.97-1.61 wt.% and 0.04-0.35 wt.%, respectively; Table 8), matrix in Sahara 00182 contains 5.75 wt.% CaO and 2.50 wt.% S (Smith et al., 2004).

5.3.3 Anticipated characteristics of unmetamorphosed, yet to be detected samples

Since all investigated CL meteorites are affected by thermal metamorphism (petrologic types 3.9 to 4; Table 2) the question remains how unmetamorphosed samples might look like. It cannot be ruled out that such samples are hidden among the tangled mass of CV_{red} and CR chondrites from Northwest Africa (NWA) and other dense collection areas. On a first glance, those samples would appear unusual due to their very high chondrule abundances and the correspondingly low amounts of fine-grained matrix (Table 2). Depending on the weathering grade, they would more or less stand out against CV_{red} chondrites by their high metal content and high magnetic susceptibility (Table 3). The O isotopic compositions would plot on the CCAM line, within the range of CV-CK chondrites or to the

direction of lighter isotopic compositions (Fig. 12). In the end, unmetamorphosed CL chondrites would be definitely uncovered by their characteristic depletions of volatile lithophile and chalcophile elements (Figs. 9, 10), and their Ti and Cr isotopic compositions (Fig. 12b).

5.4 Relationship between CL chondrites and CV and CK chondrites

The recognition of a further distinct carbonaceous chondrite group raises questions about how the characteristics of each of these groups was initially established. Oxygen and Cr isotopic data suggest a relationship between the CL chondrites and CV and CK chondrites. Perhaps their parent bodies formed in a similar nebular region (heliocentric distance) distinct from those of the other carbonaceous chondrite groups. Compared to CV and CK asteroids, the CL asteroid(s) obviously formed from a distinct mix of components, with higher amounts of chondrules and lower amounts of CAIs and matrix. The low matrix content may indicate a correspondingly low amount of co-accreted water ice which led to more reducing conditions during thermal metamorphism.

However, most CV chondrites are of low petrologic type (3.1-3.6; e.g. Bonal et al., 2006), which is in strong contrast to CK and CL chondrites. Most CK chondrites are of petrologic types 4 to 6 and all yet identified members of the CL group are of petrologic types 3.9 to 4 (Table 2). One explanation for these differences is a possible bias of material delivery to Earth by secondary parent bodies, which are in a suitable resonance position just by chance. Greenwood et al. (2020) discuss the relationship between primary and secondary parent bodies, where the latter derived from the former through impact break-up. By this process, secondary bodies form, which do not fully represent the material of the primary body. Even if all primary bodies would have had a similar, for example, onion shell structure of petrologic types (type 6 in the interior, types 5-3 in the outer layers), secondary fragments would mostly consist of material with a restricted range of petrologic types. These types would be overrepresented in our collections, if such secondary parent bodies are the main source of a given meteorite group (e.g., CL chondrites) due to their favorite resonance position.

6. SUMMARY AND CONCLUSIONS

The five ungrouped carbonaceous chondrites Coolidge, Loongana 001, LoV 051, NWA 033, and NWA 13400 can be grouped together to establish the new Loongana (CL) group of carbonaceous chondrites. The results of this study show that CL chondrites are characterized by:

1. Lithophile element ratios (e.g., Al/Mg, Si/Mg) within the range of other carbonaceous chondrite groups
2. Fe-Ni metal abundances considerably higher than for CV, but similar to CR chondrites
3. Chondrule size-frequency distributions similar to CV, but dissimilar to CR chondrites
4. Mean CAI abundances of ~1.4 vol%, i.e., lower than in CV, but much higher than in CR chondrites
5. Very low amounts of matrix (17-21 vol%), the lowest among the main carbonaceous chondrite groups (CI, CM, CO, CV, CR, CK)

6. Nearly equilibrated olivine with mean fayalite (Fa) values between 12.5 mol% (Loongana) and 14.7 mol% (NWA 13400) as a metamorphic effect
7. Lower Al_2O_3 and higher MgO and Cr_2O_3 concentrations in matrix compared to matrix in CV, CK, and CR chondrites, as a possible metamorphic effect
8. Considerable bulk depletion of volatile elements (Mn, Na, K, Rb, Cs, Zn, Se, Te, Pb, Tl) compared to all other main carbonaceous chondrite groups, reflecting the very low matrix abundance.
9. Bulk O isotope compositions plotting along the CCAM line ($\Delta^{17}O$ -3.96 to -5.47‰), partly overlapping with the CV and CK chondrite field but including samples that are ^{16}O-enriched
10. Unique positions in the $\epsilon^{54}Cr$-$\epsilon^{50}Ti$ isotope plot, with $\epsilon^{54}Cr$ values similar to CV, CK, and CO, but $\epsilon^{50}Ti$ values similar to CR chondrites.

Loongana-type (CL) chondrites show many similarities to CV and CK chondrites and may have accreted from a similar nebular reservoir, which, however, was characterized by much lower matrix and CAI abundances. The CL chondrites also display some similarities to CR chondrites (e.g., average magnetic susceptibility), but these groups are not related, as is evident from their different O and Cr isotopic compositions (Figs. 11, 12a) and Ti (Fig. 13b), and their different frequency distributions of apparent chondrule sizes (Table 7, Fig. 5).

One of the remaining key questions is whether unidentified or misidentified CL members of lower petrologic types are hidden in our collections, possibly among the large number of CV_{red} and CR chondrites from hot and cold deserts. Such samples would be important to investigate the pristine state of these meteorites and their components.

ACKNOWLEDGEMENTS

We thank Jemma Davidson, Herbert Palme, and Alan Rubin for their constructive reviews and Liping Qin for her editorial efforts. Furthermore, we thank Jutta Zipfel (Senckenberg Forschungsinstitut und Naturmuseum, Frankfurt, Germany) and Mirko Graul (Bernau, Germany) for providing samples of Loongana 001 and NWA 13400, respectively. This work was supported by the Deutsche Forschungsgemeinschaft (DFG, German Research Foundation), grant number ME 1115/10-1 and Project-ID 263649064 – TRR 170. This is TRR 170 pub. no. 128.

REFERENCES

Alexander C. M. O'D. (2019) Quantitative models for the elemental and isotopic fractionations in chondrites: The carbonaceous chondrites. *Geochim. Cosmochim. Acta* **254**, 277-309.

Alexander C. M. O'D., Greenwood R. C., Bowden R., Gibson J. M., Howard K. T. and Franchi I. A. (2018) A multi-technique search for the most primitive CO chondrites. *Geochim. Cosmochim. Acta* **221**, 406-420.

1064 Barosch J., Hezel D. C., Ebel D. S. and Friend P. (2019) Mineralogically zoned chondrules in ordinary
1065 chondrites as evidence for chondrule open system behavior. *Geochim. Cosmochim. Acta* **249**, 1–
1066 16.
1067 Barosch J., Hezel D. C., Sawatzki L., Halbauer L. and Marrocchi Y. (2020) Sectioning effects of
1068 porphyritic chondrules: implications for the PP/POP/PO classification and correcting modal
1069 abundances of mineralogically zoned chondrules. *Meteorit. Planet. Sci*. **55**, 993-999.
1070 Barrat J.-A., Zanda B., Moynier F., Bollinger C., Liorzou C. and Bayon G. (2012) Geochemistry of CI
1071 chondrites: major and trace elements, and Cu and Zn Isotopes. *Geochim. Cosmochim. Acta* **83**,
1072 79–92.
1073 Bence A. E. and Albee A. L. (1968) Empirical correction factors for the electron micro-analysis of
1074 silicates and oxides. *J. Geol.* **76**, 382–403.
1075 Bischoff A., Palme H., Ash R. D., Clayton R. N., Schutz L., Herpers U., Stöffler D., Grady M. M.,
1076 Pillinger C. T., Spettel B., Weber H., Grund T., Endreß M. and Weber D. (1993) Paired Reanazzo-
1077 type (CR) carbonaceous chondrites from the Sahara. *Geochim. Cosmochim. Acta* **57**, 1587-1603.
1078 Bonal L., Quirico E., Bourot-Denise M. and Montagnac G. (2006). Determination of the petrologic type
1079 of CV3 chondrites by Raman spectroscopy of included organic matter. *Geochim. Cosmochim. Acta*
1080 **70**, 1849-1863.
1081 Bonal L. Gattacceca J., Garenne A., Eschrig J., Rochette P. and Krämer Ruggiu L. (2020) Water and
1082 heat: new constraints on the evolution of the CV chondrite parent body. *Geochim. Cosmochim.*
1083 *Acta* **276**, 363-383.
1084 Braukmüller N., Wombacher F., Hezel D. C., Escoube R. and Münker C. (2018) The chemical
1085 composition of carbonaceous chondrites: Implications for volatile element depletion,
1086 complementarity and alteration. *Geochim. Cosmochim. Acta* **239**, 17-48.
1087 Burkhardt C., Hi. R. C., Kleine T. and Bourdon B. (2014) Evidence for Mo isotope fractionation in the
1088 solar nebula and during planetary differentiation. *Earth Planet. Sci. Lett.* **391**, 201-211.
1089 Burkhardt C., Dauphas N., Tang H., Fischer-Gödde M., Qin L., Chen J. H., Rout S. R., Pack A., Heck
1090 P. R. and Papanastassiou D. A. (2017) In search of the Earth-forming reservoir: Mineralogical,
1091 chemical, and isotopic characterizations of the ungrouped achondrite NWA 5363/NWA 5400 and
1092 selected chondrites. *Meteorit. Planet. Sci*. **52**, 807-826.
1093 Burkhardt C., Dauphas N., Hans U., Bourdon B. and Kleine T. (2019) Elemental and isotopic variability
1094 in solar system materials by mixing and processing of primordial disk reservoirs. *Geochim.*
1095 *Cosmochim. Acta* **261**, 145–170.
1096 Choe W. H., Huber H., Rubin A. E., Kallemeyn G. W. and Wasson J. T. (2010) Compositions and
1097 taxonomy of 15 unusual carbonaceous chondrites. *Meteorit. Planet. Sci*. **45**, 531-554.
1098 Clayton R. N. and Mayeda T. K. (1999). Oxygen isotope studies of carbonaceous chondrites.
1099 *Geochim. Cosmochim. Acta* **63**, 2089-2104.
1100 Dauphas N. and Schauble E. A. (2016) Mass Fractionation Laws, Mass-Independent Effects, and
1101 Isotopic Anomalies. *Annu. Rev. Earth Planet. Sci.* **44**, 709–783.
1102 Davis A. M., Zhang J., Greber N. D., Hu J., Tissot F. L. H., and Dauphas N (2018) Titanium isotopes
1103 and rare earth patterns in CAIs: evidence for thermal processing and gas-dust decoupling in the
1104 protoplanetary disk. *Geochim. Cosmochim. Acta* **221**, 275-295.

1105 Ebel D. S., Brunner C., Konrad K., Leftwich K., Erb, I., Lu M., Rodriguez H., Crapster-Pregont E. J.,
1106 Friedrich J. M., and Weisberg M. K. (2016) Abundance, major element composition and size of
1107 components and matrix in CV, CO and Acfer 094 chondrites. *Geochim. Cosmochim. Acta* **172**,
1108 322-356.
1109 Ebert S., Render J., Brennecka G. A., Burkhardt C., Bischoff A., Gerber S., Kleine T. (2018) Ti isotopic
1110 evidence for a non-CAI refractory component in the inner Solar System. *Earth Planet. Sci. Lett.*
1111 **498**, 257-265.
1112 Eisenhour D. D. (1996) Determining chondrule size distributions from thin-section measurements.
1113 *Meteorit. Planet. Sci.* **31**:243-248.
1114 Feldstein S. N., Jones R. H. and Papike J. J. (2001) Disequilibrium partial melting experiments on the
1115 Leedey L6 chondrite: Textural controls on melting processes. *Meteorit. Planet. Sci.* **36**,1421–1441.
1116 Friend P., Hezel D. C. and Mucerschi D. (2016) The conditions of chondrule formation, Part II: Open
1117 system. *Geochim. Cosmochim. Acta* **173**, 198–209.
1118 Gattacceca J., Suavet C., Rochette P., Weiss B.P., Winklhofer M., Uehara M. and Friedrich J. (2014)
1119 Metal phases in ordinary chondrites: magnetic hysteresis properties and implications for thermal
1120 history. *Meteorit. Planet. Sci*. **49**, 652-676.
1121 Gattacceca J., Bonal L., Sonzogni C. and Longerey J. (2020) CV chondrites: more than one parent
1122 body. *Earth Planet. Sci. Lett.* **547**, 116467.
1123 Greenwood R. V., Franchi I. A., Kearsley A. T. and Alard O. (2010) The relationship between CK and
1124 CV chondrites. *Geochim. Cosmochim. Acta* **74**, 1684-1705.
1125 Greenwood R. C., Burbine T. H., Miller M. F. and Franchi I. A. (2017) Melting and differentiation of
1126 early-formed asteroids: The perspective from high precision oxygen isotope studies: *Chemie der*
1127 *Erde-Geochemistry* **77**, 1-43.
1128 Greenwood R.C., Burbine T. H. and Franchi I.A. (2020) Linking asteroids and meteorites to the
1129 primordial planetesimal population *Geochim. Cosmochim. Acta* **277**, 377-406.
1130 Griffin W. L., Powell W. J., Pearson N. J. and O'Reilly S.Y. (2008) GLITTER: data reduction software
1131 for laser ablation ICP-MS, in Sylvester, P., ed*., Laser Ablation ICP-MS in the Earth Sciences:*
1132 *Current Practices and Outstanding Issues*, Mineralogical Association of Canada. Short Course
1133 Series **40**, 308-311.
1134 Guimon R. K., Symes S. J. K., Sears D. W. G. Sears and Benoit P (1995) Chemical and physical
1135 studies of type 3 chondrites XII: The metamorphic history of CV chondrites and their components.
1136 *Meteorit. Planet. Sci*. **30**, 704-714.
1137 Hezel D. C. (2010) A mathematica code to produce phase maps from two element maps*. Computers*
1138 *& Geosciences* **36**, 1097–1099.
1139 Hellmann J. L., Hopp T., Burkhardt C. and Kleine T. (2020) Origin of volatile depletion among
1140 carbonaceous chondrites. *Earth Planet. Sci. Lett.* **549**; 116508.
1141 Hezel D. C. and Palme H. (2008) Constraints for chondrule formation from Ca-Al distribution in
1142 carbonaceous chondrites. *Earth Planet. Sci. Lett.* **265**, 716-725.
1143 Hezel D. C., Russell S. S., Ross A. J., and Kearsley A. T. (2008) Modal abundances of CAIs:
1144 Implications for bulk chondrite element abundances and fractionations. *Meteorit. Planet. Sci*. **43**,
1145 1879-1894.

Hutchison R. (2004) *Meteorites - A petrologic, chemical and isotopic synthesis*. In Cambridge Planetary Science (ed. Bagenal F., Jewitt D., Murray C., Bell J., Lorenz R., Nimmo F., and Russell S. Cambridge, UK: Cambridge University Press. 506 p.

Jacquet E. (2021) Collisions and compositional variability in chondrule-forming events. *Geochim. Cosmochim. Acta* **296**, 18-37.

Jarosewich E. (2006) Chemical analysis of meteorites at the Smithsonian Institution: An update. *Meteorit. Planet. Sci*. **41**, 1381-1382.

Jarosewich E., Clarke R. S., Jr. and Barrows J. N. (1987) The Allende meteorite reference sample. In: *The Allende meteorite reference sample* (eds. E. Jarosewich, R. S. Clark, and J. N. Barrows), Smiths. Inst. Press, Washington D.C., pp. 1-12.

Jochum K. P., Nohl U., Herwig K., Lammel E., Stoll B. and Hofmann, A.W. (2005) GeoReM: A New Geochemical Database for Reference Materials and Isotopic Standards. *Geostandards and Geoanalytical Research* **29-3**, 333-338.

Jones R. H., Grossman J. N. and Rubin A. E. (2005). Chemical, mineralogical and isotopic properties of chondrules: Clues to their origin. In *Chondrites and the Protoplanetary Disk* (eds. A.N. Krot, E.R.D. Scott, and B. Reipurth). Astronomical Society of the Pacific Conference Series **341**, 251-285.

Kallemeyn (1987) Compositional comparisons of metamorphosed carbonaceous chondrites. Mem. Natl. Inst. Polar Res., Spec. Issue, **46**, 151-161.

Kallemeyn G. W. and Rubin A. (1995) Coolidge and Loongana 001: A new carbonaceous chondrite grouplet. *Meteoritics* **30**, 20-27.

Kallemeyn G. W. and Wasson J. T. (1981) The compositional classification of chondrites: I. The carbonaceous chondrite groups. *Geochim. Cosmochim. Acta* **45**, 1217-1230.

Kallemeyn G. W. and Wasson J. T. (1982) The compositional classification of chondrites: III. Ungrouped carbonaceous chondrites. *Geochim. Cosmochim. Acta* **46**, 2217-2228.

Kallemeyn G. W., Rubin A. E. and Wasson J. T. (1991) The compositional classification of chondrites: V. The Karoonda (CK) group of carbonaceous chondrites. *Geochim. Cosmochim. Acta* **55**, 881-892.

Kallemeyn G. W., Rubin A. E. and Wasson J. T. (1994) The compositional classification of chondrites: VI. The CR carbonaceous chondrite group. *Geochim. Cosmochim. Acta* **58**, 2873-2888.

King A. J., Bates H. C., Krietsch D., Busemann H., Clay P. I., Schofield P. F. and Russell S. S. (2019) The Yamato-type (CY) carbonaceous chondrite group: Analogues for the surface of asteroid Ryugu? *Geochemistry* **79**, 125531.

Kleine T., Budde G., Burkhardt C., Kruijer T. S., Worsham E. A., Morbidelli A. and Nimmo F. (2020) The Non-carbonaceous-Carbonaceous meteorite dichotomy. *Space Sci. Rev*. **216**:55.

Knab H.-J. (1981) The distributions of trace elements in carbonaceous chondrites. *Geochim. Cosmochim. Acta* **45**, 1563-1572.

Krot, A. N., Keil, K., Scott, E. R. D., Goodrich, C. A. and Weisberg, M. K. (2014) Classification of meteorites and their genetic relationships. *In: Meteorites and Cosmochemical Processes*, Treatise on Geochemistry (Second Edition; ed. A. M. Davis). Elsevier, Vol. 1, pp.1-63.

Krot A. N. (2019) Refractory inclusions in carbonaceous chondrites: Records of early solar system processes. *Meteorit. Planet. Sci*. **54**, 1647-1691.

Lauretta D. S., Nagahara H. and Alexander C. M. O`D. (2006) Petrology and origin of ferromagnesian silicate chondrules. In: *Meteorites and the early solar system II*, edited by Lauretta D. S. and McSween H. Y. Tucson: The University of Arizona Press: 431-459.

Lodders K. (2003) Solar system abundances and condensation temperatures of the elements. *Astroph. J.* **591**, 1220-1247.

Lodders K., Palme H. and Gail H. P. (2009) *Abundances of the elements in the solar system.* In: Landolt-Börnstein, New Series, vol. VI/4B (ed. J. E. Trümper). Springer, pp. 560-630.

Mallozzi L., MacPherson G. J., Corrigan C. M., Irving A. J. and Pitt D. (2018) Northwest Africa 8418: A CV4 chondrite, with new insight into secondary processes on the CV parent body (abstract). In: *30th Lunar and Planetary Science Conference*, #2555.

MBDB (Meteoritical Bulletin Database) https://www.lpi.usra.edu/meteor/.

McCoy-West A. J., Millet M.-A. and Burton K. Y. (2017) The neodymium stable isotope composition of the silicate Earth and chondrites. *Earth Planet. Sci. Lett.* **480**, 121-132.

McSween H. Y. Jr. (1977a) Petrographic variations among carbonaceous chondrites of the Vigarano type. *Geochim. Cosmochim. Acta* **41**, 1777-1790.

McSween H. Y. Jr. (1977b) Chemical and petrographic constraints on the origin of chondrules and inclusions in carbonaceous chondrites. *Geochim. Cosmochim. Acta* **41**, 1843-1860.

McSween H. Y. Jr. and Richardson S. M. (1977) The composition of carbonaceous chondrite matrix. *Geochim. Cosmochim. Acta* **41**, 1145-1161.

Metzler K. (2012) Ultrarapid chondrite formation by hot chondrule accretion? Evidence from unequilibrated ordinary chondrites. *Meteorit. Planet. Sci*. **47**, 2193-2217.

Metzler K. (2018) From 2D to 3D chondrule sizes: Some empirical ground truths. *Meteorit. Planet. Sci*. **53**, 1489-1499.

Metzler K., Hezel D. C., and Nellesen J. (2019) Various size-sorting processes for millimeter-sized particles in the Sun´s protoplanetary disk? Evidence from chondrules in ordinary chondrites. *Astroph. J.* **887**, 230.

Matza S. D. and Lipschutz M. E. (1977) Volatile/mobile trace elements in Karoonda (C4) chondrite. *Geochim. Cosmochim. Acta* **41**, 1398-1401.

Miller M. .F., Franchi I. A., Sexton A. S. and Pillinger C. T. (1999). High precision $\Delta^{17}O$ isotope measurements of oxygen from silicates and other oxides: Methods and applications. *Rapid Comm. Mass Spec. **13***, 1211-1217.

Millet M.-A. and Dauphas N. (2014) Ultra-precice titanium stable isotope measurements by double-spike high resolution MC-ICP-MS. *J. Analyt. Atom. Spectr*. **29,** 1444-1458.

Mougel B., Moynier F. and Göpel C. (2018) Chromium isotopic homogeneity between the Moon, the Earth, and enstatite chondrites. *Earth Planet. Sci. Lett*. **481**, 1–8.

Noguchi T. (1994) Petrology and mineralogy of the Coolidge meteorite (CV4). *Proc. NIPR Symp. Antarct. Meteorites* **7**, 42-72.

Palme H. and Rammensee W. (1981) The cosmic abundance of molybdenum. *Earth Planet. Sci. Lett. **55**, 356-362.*

Pourkhorsandi H., D'Orazio M., Rochette P., Valenzuela M., Gattacceca J., Mirnejad H., Sutter B., Hutzler A., and Aboulahris M. (2017a) Modification of REE distribution of ordinary chondrites from Atacama (Chile) and Lut (Iran) hot deserts: Insights into the chemical weathering of meteorites. *Meteorit. Planet. Sci*. **52**, 1843-1858.

Pourkhorsandi H., Gattacceca J., Devouard B., D'Orazio M., Rochette P., Beck P., Sonzogni C., and Valenzuela M. (2017b) The ungrouped chondrite El Médano 301 and its comparison with other reduced ordinary chondrites. *Geochim. Cosmochim. Acta* **218**, 98-113.

Qin L., Alexander C. M. O., Carlson R. W., Horan M. F. and Yokoyama T. (2010) Contributors to chromium isotope variation of meteorites. *Geochim. Cosmochim. Acta* **74**, 1122–1145.

Render J., Ebert S., Burkhardt C., Kleine T. and Brennecka G. A. (2019) Titanium isotopic evidence for a shared genetic heritage of refractory inclusions from different carbonaceous chondrites. *Geochim. Cosmochim. Acta* **254**, 40–53.

Rochette P., Gattacceca J., Bonal L., Bourot-Denise M., Chevrier V., Clerc J.-P., Consolmagno G., Folco L., Gounelle M., Kohout T., Pesonen L., Quirico E., Sagnotti L. and Skripnik A. (2008) Magnetic Classification of Stony Meteorites: 2. Non-Ordinary Chondrites, *Meteorit. Planet. Sci*. **43**, 959-980.

Rubin A. E. and Wasson J. T. (2005) Non-spherical lobate chondrules in CO3.0 Y-81020: General implications for the formation of low-FeO porphyritic chondrules in CO chondrites. *Geochim. Cosmochim. Acta* **69**, 211-220.

Sanborn M. E., Wimpenny J., Williams C. D., Yamakawa A., Amelin Y., Irving A. J. and Yin Q.-Z. (2019) Carbonaceous achondrites Northwest Africa 6704/6693: Milestones for early Solar System chronology and genealogy. *Geochim. Cosmochim. Acta* **245**, 577–596.

Schrader D. L., Franchi I. A., Connolly H. C., Greenwood R. C., Lauretta D. S. and Gibson J. M. (2011) The formation and alteration of the Renazzo-like carbonaceous chondrites I: Implications of bulk-oxygen isotopic composition. *Geochim. Cosmochim. Acta* **75**, 308-325.

Schrader D. L., Davidson J., Greenwood R. C.; Franchi I. A. and Gibson J. M. (2014) A water-ice rich minor body from the early Solar System: The CR chondrite parent asteroid. *Earth Planet. Sci. Lett*. **407**, 48-60.

Scott E. R. D. and G. J. Taylor (1985) Petrology of types 4-6 carbonaceous chondrites. Proc. 15th Lunar Planet Sci. Conf., *JGR* **90**, Suppl., C699-C709.

Schneider J. M., Burkhardt C., Marrocchi Y., Brennecka A. and Kleine T. (2020) Early evolution of the solar accretion disk inferred from Cr-Ti-O isotopes in individual chondrules. *Earth Planet. Sci. Lett*. **551**, 116585.

Simon J. I., Cuzzi J. N., McCain K. A., Cato M. J., Christoffersern P. A., Fisher K. R., Srinivasan P., Tait A. W., Olson D. M., Scargle J. D. (2018) Particle size distributions in chondritic meteorites: Evidence for pre-planetesimal histories. *Earth Planet. Sci. Lett*. **494**, 69-82.

Smith D. L., Russell S. S., Gounelle M., Greenwood R. C. and Franchi I. A. (2004) NWA 1152 and Sahara 00182: New primitive carbonaceous chondrites with affinities to the CR and CV groups. *Meteorit. Planet. Sci*. **39**, 2009-2032.

1266 Starkey N. A., Jackson C. R. M., Greenwood R. C., Parman S., Franchi I. A., Jackson M., Fitton J. G.,
1267 Stuart F.M., Kurz M. and Larsen L.M. (2016). Triple oxygen isotopic composition of the high
1268 3He/4He mantle. *Geochim. Cosmochim. Acta* **176**, 227-238.
1269 Stöffler D., Keil K. and Scott E. R. D. (1991) Shock metamorphism of ordinary chondrites. *Geochim.*
1270 *Cosmochim. Acta* **55**, 3845-3867.
1271 Stöffler, D., Hamann C. and Metzler K. (2018) Shock metamorphism of planetary silicate rocks and
1272 sediments: Proposal for an updated classification system. *Meteorit. Planet. Sci*. **53**, 5-49.
1273 Stracke, A., Palme, H., Gellissen, M., Münker, C., Kleine, T., Birbaum, K., Günther, D., Bourdon, B.,
1274 and Zipfel, J. 2012. Refractory element fractionation in the Allende meteorite: Implications for solar
1275 nebula condensation and the chondritic composition of planetary bodies. *Geochim. Cosmochim.*
1276 *Acta* **85**, 114–41.
1277 Teitler S.A., Paque J.M., Cuzzi J.N., and Hogan R.C. (2010) Statistical tests of chondrule sorting.
1278 *Meteorit. Planet. Sci.* **45**, 1124–1135.
1279 Torrano Z. , Davidson J., and Wadhwa M. (2020) A reclassification of Northwest Africa 2900 from CV3
1280 to CK3 chondrite. *Meteorit. Planet. Sci.* **55**, 2539-2550.
1281 Trinquier A., Birck J. and Allegre C. J. (2007) Widespread ^{54}Cr heterogeneity in the inner solar system.
1282 *Astroph. J.* **655**, 1179–1185.
1283 Trinquier A., Elliott T., Ulfbeck D., Coath C., Krot A. N. and Bizzarro M. (2009) Origin of
1284 nucleosynthetic isotope heterogeneity in the solar protoplanetary disk. *Science* **324**, 374–376.
1285 Ushikubo T., Kimura M., Kita N. T. and Valley J.W. (2011) Primordial oxygen isotope reservoirs of the
1286 solar nebula recorded in chondrules in Acfer 094 carbonaceous chondrite. *Geochim. Cosmochim.*
1287 *Acta* **90**, 242-264.
1288 Van Schmus W. R. (1969) Mineralogy, petrology and classification of types 3 and 4 carbonaceous
1289 chondrites. In *Meteorite Research* (ed. P. M. Millman), pp. 480 -491. Reidel.
1290 Wang Z., Becker H. and Wombacher F. (2014) Mass fractions of S, Cu, Se, Mo, Ag, Cd, In, Te, Ba,
1291 Sm, W, Tl and Bi in geological reference materials and selected carbonaceous chondrites
1292 determined by isotope dilution ICP-MS. *Geostand. Geoanal. Res.* **39**, 185–208.
1293 Warren P. H. (2011) Stable isotopes and the noncarbonaceous derivation of ureilites, in common with
1294 nearly all differentiated planetary materials. *Geochim. Cosmochim. Acta* **75**, 6912-6926.
1295 Weckwerth G. (2014) Instrumental neutron activation analyses of the most Earth-like meteorites. *J.*
1296 *Radioanal. Nucl. Chem*. **299**, 221-228.
1297 Weckwerth G. and Weber D. (1998) The 3rd member of the Coolidge type grouplet: implications for
1298 element fractionations trends in carbonaceous chondrites (abstract). In: *29th Lunar Planet Sci.*
1299 *Conf.*, # 1739.
1300 Weckwerth G., Wolf D., Bartoschewitz R. and Ackermand D. (2001) NWA 779, a new CV-chondrite
1301 with relations to the Coolidge grouplet? (abstract). In: *64th Ann. Meet. Meteorit. Soc.*, #5378.
1302 Weisberg M. K. (2001) Sahara 00182, the first CR3 chondrite and formation of multi-layered
1303 chondrules (abstract). *Meteorit. Planet. Sci*. **36**, A222–A223.
1304 Weisberg M.K., Prinz M., Clayton R.N., and Mayeda T.K. (1997) CV3 chondrites: three subgroups, not
1305 two (abstract). *Meteorit. Planet. Sci*. **32**, A138–A139.

1306 Weisberg M. K., McCoy T. J. and Krot A. N. (2006) Systematics and evaluation of meteorite
1307 classification. In *Meteorites and the early solar system II* (ed. D. S. Lauretta and H. Y. McSween
1308 jr.), University of Arizona Press. pp. 679-712.
1309 Wlotzka F. (1993) A weathering scale for the ordinary chondrites (abstract). *Meteoritics* **28**, 460.
1310 Wolf D. and Palme, H. 2001. The solar system abundances of phosphorus and titanium and the
1311 nebular volatility of phosphorus. *Meteoritics* **36**, 559–571.
1312 Wood B. J., Smythe D. J. and Harrison T. (2019) The condensation temperatures of the elements: A
1313 reappraisal. *Am. Min.* **104**, 844-856.
1314 Wulf A. V., Palme H. and Jochum K. P. (1995) Fractionation of volatile elements in the early solar
1315 system: evidence from heating experiments on primitive meteorites. *Planet. Space Sci.* **43**, 451-
1316 468.
1317 Yamakawa A., Yamashita K. Makishima A. and Nakamura E. (2009) Chemical separation and mass
1318 spectrometry of Cr, Fe, Ni, Zn, and Cu in terrestrial and extraterrestrial material using thermal
1319 ionization mass spectrometry. *Anal Chem.* **81**, 23, 9787-9794.
1320 Young E. D. and Russell S. S. (1998) Oxygen reservoirs in the early solar nebula inferred from an
1321 Allende CAI. *Science* **282**, 1874–1877.
1322 Zhang J., Dauphas N., Davis A. M. and Pourmand A. (2011) A new method for MC-ICP-MS
1323 measurement of titanium isotopic composition: Identification of correlated isotope anomalies in
1324 meteorites. *J. Anal. At. Spectrom.* **26**, 2197.
1325 Zhang J., Dauphas N., Davis A. M., Leya I. and Fedkin A. (2012) The proto-Earth as a significant
1326 source of lunar material. *Nat. Geosci.* **5**, 251–255.
1327

TABLES

Table 1: Sample allocation, weight, and designation of the investigated (sub)samples of CL chondrites.

	Coolidge	Loongana 001	LoV 051	NWA 033	NWA 13400
Powder sample, total (mg)	559	565	513	598	610
ICP-MS					
University of Münster, Inst. f. Planetologie					
Sample powder (mg)	128	137	81	163	178
ICP-MS					
University of Münster, Inst. f. Mineralogie					
Sample powder (mg)	86	86	87	84	86
Laser fluorination					
Open University, Milton Keynes					
Sample powder (mg)	10	10	15	10	10
XRF					
University of Cologne					
Sample powder (mg)	131	130	130	134	135
SEM-EDX, Polarizing microscopy					
University of Münster, Inst. f. Planetologie					
Polished thin section numbers (size; mm^2)	-K-397-a-1 (52)	-F-a-1 (54)	-MS-a-1 (76)	PL-00027 (112)	-MS-a-1 (361)
LA-ICP-MS					
University of Münster, Inst. f. Mineralogie					
Thick section numbers (size; mm^2)	-K-397-a (52)	-F-a (44)	-MS-a (76)	-MS-a (126)	-MS-a (152)
Sample source	1	2	3	4	5

1: University of Cologne, Inst. f. Geologie und Mineralogie, Germany; 2: Senckenberg Forschungsinstitut und Naturmuseum, Frankfurt, Germany; 3: CEREGE (CNRS/University Aix-Marsaille), France; 4: University of Münster, Inst. f. Planetologie, Germany; 5: Mirko Graul, Bernau, Germany.

Table 2: Classification details for the investigated CL chondrites and modal abundances of their lithologic components.

	Coolidge	Loongana 001	LoV 051	NWA 033	NWA 13400
Proposed petrologic type[1]	4	4	3.9	4	3.9
PMD Fa[2]	2.5	3.1	9.2	4.4	8.9
Mean Fa±s.d.	14.5±0.4	12.5±0.4	12.8±1.2	13.5±0.6	14.7±1.3
Mean Fs±s.d.[3]	9.4±3.9	10.4±2.1	10.2±3.3	7.9±3.1	6.6±3.7
Shock stage[4]	C-S2	C-S2	C-S2	C-S2	C-S2
Weathering grade[5]	W2	W3	W1/2	W3/4	W2/3
Mean apparent chondrule size (µm)[6]	404	414	476	455	477
Modal abundances (vol%)					
Chondrules + fragments	79	67	78	72	76
Matrix	18	20	17	21	17
Inter-chondrule metal/sulfide[7]	3	5	5	6	6
CAIs[8]	0.1	8.0	0.4	0.9	1.0

[1] According to Hutchison (2004); [2] PMD Fa: Percentage mean deviation of fayalite values (mol%) in olivine grains (see also Table 4); [3] Fs: ferrosilite values (mol%) in low-Ca pyroxene (see also Table 5); [4] according to Stöffler et al. (2018); [5] according to Wlotzka (1993); [6] for details see Table 7; [7] partly/largely replaced by oxidation products; [8] Highly variable due to small thin section sizes (see Hezel et al., 2008). s.d.: 1 standard deviation.

1342 **Table 3.** Magnetic properties of the investigated CL chondrites, compared to literature data for other
1343 groups of carbonaceous chondrites (CV_{red}, CV_{oxA}, CV_{oxB}, CR). χ: magnetic susceptibility; sd: standard
1344 deviation; M_S: saturation magnetization; M_{RS}: saturation remanent magnetization; B_C: coercive force;
1345 B_{CR}: remanent coercive force.

Meteorite	logχ	sd	n or studied mass (g)	M_S (Am^2/kg)	M_{RS} (Am^2/kg)	B_C (mT)	B_{CR} (mT)	M_{RS}/M_S	B_{CR}/B_C	n or studied mass (mg)
Coolidge	4.94		23.4 g							
Loongana 001	4.97		4.3 g							
LoV 051	5.24		15.0 g	32.3	0.50	3.08	18.8	$1.55x10^{-2}$	6.10	205 mg
NWA 033	4.69		22.7 g							
NWA 13400	4.78		4.2 g	9.78	1.23	11.4	21.4	$1.26x10^{-1}$	1.88	370 mg
CV_{red}	4.43	0.22	10	8.03±4.40	0.58±0.26	16.9±7.0	66.1±37.2	$7.22x10^{-2}$	3.91	10
CV_{oxA}	3.62	0.27	11	0.69±0.37	0.053±0.018	15.4±0.6	64.6±12.1	$7.68x10^{-2}$	4.19	11
CV_{oxB}	4.39	0.27	10	5.52±2.78	1.19±0.49	23.9±5.5	44.8±7.0	$2.16x10^{-1}$	1.87	10
CR	5.04	0.12	14	47.3	0.43	1.33	16.1	$9.09x10^{-3}$	12.11	259 mg

1346 Susceptibility data for CV chondrites: Rochette et al. (2008) and Bonal et al. (2020) with the addition of Catalina 300 (CV_{OxB})
1347 from Gattacceca et al. (2020). Susceptibility data for CR chondrites, Loongana, and Coolidge: Rochette et al. (2008). M_S and
1348 M_{RS} data for CV chondrites: Bonal et al. (2020).
1349

Table 4. Mean chemical composition of olivine in the investigated CL chondrites (EMPA; wt.%).

	Coolidge	Loongana 001	LoV 051	NWA 033	NWA 13400
SiO_2	40.9±0.2	41.1±0.3	40.5±0.3	40.7±0.2	40.2±0.4
TiO_2	0.07±0.05	0.06±0.04	0.04±0.04	0.05±0.03	0.03±0.03
Al_2O_3	0.05±0.08	0.02±0.04	0.02±0.02	0.03±0.04	0.03±0.05
Cr_2O_3	0.09±0.18	0.04±0.03	0.05±0.04	0.04±0.03	0.05±0.05
FeO	13.8±0.4	11.9±0.4	12.5±1.1	12.8±0.6	14.1±1.2
MnO	0.23±0.03	0.23±0.03	0.24±0.03	0.24±0.04	0.23±0.05
MgO	45.8±0.3	47.0±0.4	47.5±0.8	46.2±0.5	45.8±1.1
CaO	0.03±0.04	0.02±0.02	0.01±0.01	0.02±0.02	0.04±0.04
Na_2O	0.01±0.01	0.01±0.02	0.01±0.02	0.01±0.02	0.01±0.02
NiO	0.02±0.02	0.02±0.02	0.02±0.02	0.02±0.02	0.03±0.03
Total	101.00	100.40	100.89	100.11	100.52
Fa	*14.5±0.4 (12.8-15.1)*	*12.5±0.4 (11.0-13.2)*	*12.8±1.2 (10.5-15.0)*	*13.5±0.6 (10.1-14.5)*	*14.7±1.3 (10.2-16.0)*
FeO/MnO	*60*	*52*	*52*	*53*	*61*
n	*44*	*49*	*47*	*46*	*30*

Fa: Fayalite content in olivine (mol%); ±: 1 standard deviation; Numbers in parenthesis: range of measured values.

Table 5. Mean chemical composition of low-Ca pyroxene in the investigated CL chondrites (EMPA; wt.%).

	Coolidge	Loongana 001	LoV 051	NWA 033	NWA 13400
SiO_2	58.5±0.7	58.2±0.8	57.6±0.7	58.4±0.9	58.0±1.0
TiO_2	0.12±0.06	0.10±0.05	0.13±0.06	0.10±0.06	0.10±0.06
Al_2O_3	0.81±0.25	0.59±0.23	0.67±0.24	0.73±0.30	0.71±0.16
Cr_2O_3	0.37±0.11	0.33±0.07	0.32±0.07	0.39±0.09	0.40±0.07
FeO	6.37±2.59	6.99±1.40	6.99±2.26	5.32±2.04	4.51±2.55
MnO	0.14±0.08	0.16±0.05	0.16±0.08	0.13±0.06	0.12±0.05
MgO	34.2±1.8	33.5±0.9	34.2±1.6	34.6±1.4	35.7±1.5
CaO	0.48±0.07	0.44±0.15	0.57±0.16	0.45±0.12	0.55±0.05
Na_2O	0.01±0.01	0.01±0.01	0.01±0.02	0.02±0.02	0.02±0.02
NiO	0.02±0.04	0.05±0.05	0.03±0.02	0.04±0.03	0.09±0.08
Total	101.02	100.37	100.68	100.18	100.20
Fs	*9.4±3.9 (1.3-14.1)*	*10.4±2.1 (6.9-14.0)*	*10.2±3.3 (2.7-14.6)*	*7.9±3.1 (3.1-15.2)*	*6.6±3.7 (1.2-15.9)*
Wo	*0.9±0.1(0.7-1.2)*	*0.9±0.3 (0.5-1.5)*	*1.1±0.3 (0.7-1.9)*	*0.9±0.2 (0.4-1.3)*	*1.0±0.1 (0.8-1.2)*
FeO/MnO	*46*	*44*	*44*	*41*	*38*
n	*27*	*24*	*45*	*49*	*20*

Fs, Wo: Ferrosilite, wollastonite content in low-Ca pyroxene (mol%); ±: 1 standard deviation; Numbers in parenthesis: range of measured values.

Table 6. Mean chemical composition of Ca-rich pyroxene in the investigated CL chondrites (EMPA; wt.%).

	Coolidge	Loongana 001	LoV 051	NWA 033	NWA 13400
SiO_2	54.6±1.1	54.2±2.1	53.7±1.2	53.9±0.7	54.3±0.9
TiO_2	1.09±0.33	0.93±0.48	0.96±0.31	1.07±0.29	1.06±0.38
Al_2O_3	2.75±1.15	3.91±2.40	3.38±1.40	3.33±1.32	2.91±0.89
Cr_2O_3	0.69±0.16	0.84±0.46	0.69±0.22	0.98±0.31	0.59±0.14
FeO	4.12±1.97	3.40±2.03	3.42±1.80	2.95±1.36	2.64±1.85
MnO	0.21±0.05	0.22±0.10	0.17±0.04	0.23±0.08	0.16±0.05
MgO	21.0±2.5	22.2±4.5	20.6±2.2	19.4±1.6	23.1±3.4
CaO	16.3±4.2	14.7±6.1	17.3±3.6	18.4±2.6	15.2±4.4
Na_2O	0.30±0.14	0.19±0.14	0.29±0.18	0.33±0.23	0.09±0.12
NiO	0.03±0.04	0.04±0.07	0.03±0.04	0.04±0.04	0.07±0.05
Total	101.09	100.63	100.54	100.63	100.12
Fs	*6.6±3.2 (1.4-10.8)*	*5.4±3.1 (1.6-9.8)*	*5.5±2.9 (1.4-12.0)*	*4.8±2.2 (0.7-8.6)*	*4.2±2.9 (0.8-10.2)*
Wo	*33.5±8.8 (18.4-43.6)*	*30.9±13.5 (12.3-43.7)*	*35.5±7.6 (16.3-45.6)*	*38.6±5.4 (27.1-49.3)*	*30.9±9.4 (10.7.1-4.6)*
FeO/MnO	*20*	*15*	*20*	*13*	*17*
n	*10*	*8*	*38*	*28*	*23*

Fs, Wo: Ferrosilite, wollastonite content in Ca-rich pyroxene (mol%); ±: 1 standard deviation; Numbers in parenthesis: range of measured values.

1364 **Table 7.** Statistics (µm) for the distributions of apparent chondrule sizes in the investigated CL
1365 chondrites, Allende (CV), and NWA 7020 (CR).

	Coolidge	Loongana 001	LoV 051	NWA 033	NWA 13400	Mean CL	*Allende* CV_{oxA}	*NWA 7020* *CR*
Mean	404 *(610)*[1]	414 *(700)*[1]	476	455	477	457	*470*	*633*
Median	270	288	403	332	342	341	*357*	*506*
StDev[2]	405	347	327	349	421	375	*366*	*468*
Skewness	2.60	2.13	2.07	1.69	2.02	2.07	*2.10*	*1.20*
Min[3]	55	75	75	65	50	50	*70*	*65*
Max[4]	2790	2295	2490	2070	2930	2930	*2670*	*2540*
n[5]	145	235	397	274	512	1563	*421*	*148*

1366 [1] Literature data (Kallemeyn and Rubin, 1995); [2] 1 standard deviation; [3] Size of the smallest chondrule; [4] Size of the largest
1367 chondrule; [5] Number of analyzed chondrules.

1368

1369

1370 **Table 8.** Bulk composition of Matrix in the investigated CL chondrites (EMPA[1]; wt.%). Literature values
1371 for other carbonaceous groups are given for comparison. Clg: Coolidge; Loo: Loongana; LoV: LoV051;
1372 033: NWA 033; 13400: NWA 13400.

	CL						CV_{red}[2]	CV_{oxA}[2]	CK	CR
	Clg	Loo	LoV	033	13400	Mean CL	Vigarano*	Allende*	Karoonda*	Renazzo*
SiO_2	30.8	27.7	30.9	29.5	32.8	30.3	31.2	30.1	34.1	36.6
TiO_2	0.10	0.13	0.13	0.11	0.18	0.13	0.10	0.10	0.55	0.08
Al_2O_3	2.01	2.18	1.56	2.04	1.41	1.84	4.70	2.48	7.63	3.10
Cr_2O_3	0.79	0.81	0.44	0.61	0.89	0.71	0.44	0.41	0.40	0.41
FeO	31.5	34.5	30.3	32.3	25.2	30.8	35.9	34.3	28.14	28.3
MnO	0.14	0.15	0.16	0.15	0.20	0.16	0.15	0.23	0.14	0.38
MgO	28.3	25.6	28.9	27.5	31.3	28.3	18.8	21.7	18.7	18.4
CaO	0.97	1.61	1.11	1.23	0.98	1.18	1.68	2.55	3.98	1.01
Na_2O	0.25	0.29	0.36	0.53	0.09	0.30	0.54	0.24	0.22	1.35
K_2O	0.03	0.03	0.03	0.04	0.03	0.03	0.06	0.01	0.13	0.19
P_2O_5	0.15	0.19	0.13	0.16	0.24	0.17	nd	nd	nd	nd
Ni	1.01	1.56	1.04	1.26	0.87	1.15	1.20	1.55	0.22	1.36
S	0.15	0.09	0.35	0.08	0.04	0.14	0.22	1.22	0.09	3.72
Total	96.20	94.84	95.41	95.51	94.23	*95.24*	*95.00*	*95.00*	*95.00*	*95.00*
n	*10*	*10*	*10*	*12*	*10*		*20*	*20*	*20*	*20*

1373 [1] defocused beam (30 µm)
1374 [2] CV subgroups: CV_{red} = reduced; CV_{oxA} = oxidized Allende-type (Weisberg et al., 1997)
1375 *McSween and Richardson (1977); *recalculated to 95.00 wt.% for comparison*
1376 nd: not determined
1377 n: number of analyzed areas
1378

Table 9. Bulk chemical composition (major and minor elements; wt.%) of the investigated CL chondrites and Allende. Literature data for Allende are given for comparison. Sample abbreviations: see Table 8.

	Lab[1]	RSD (%)[2]	Clg[3]	Loo[4]	LoV	033	13400	Mean CL	Allende[5]
SiO_2	A	< 1	33.05 *(33.59; 33.52; nd)*	34.64	33.94	34.36	34.26	34.05	34.05 *(34.3, 34.15; nd)*
TiO_2	A	< 1	0.14 *(0.14; 0.14; nd)*	0.15	0.15	0.15	0.15	0.15	0.15 *(0.15; 0.15, 0.13)*
Al_2O_3	A	< 1	3.15 *(2.83; 2.83; 3.74)*	2.91 *(3.36)*	3.20	3.07	3.11	3.09	3.20 *(3.28; 3.23, 3.15)*
Cr_2O_3	A	< 1	*0.51*[6] *(0.46; 0.43; 0.64)*	0.49 *(0.53)*	0.51	0.52	0.52	0.51	0.50 *(0.53; 0.53; 0.53)*
FeO	A	< 1	30.99 *(27.02; 27.04; 24.83)*	29.83 *(29.46)*	30.46	29.02	30.07	30.07	29.82 *(30.3; 30.31; 30.60)*
MnO	A; B	< 1; 1.3	0.15; 0.15 *(0.14; 0.14; 0.15)*	0.16; 0.16 *(0.14)*	0.14; 0.15	0.16; 0.15	0.15; 0.15	0.15	0.19; 0.19 *(0.19; 0.19; 0.19)*
MgO	A	< 1	24.52 *(24.58; 24.57; 24.87)*	25.32 *(24.04)*	25.30	25.39	24.47	25.00	24.83 *(24.6; 24.56; 24.79)*
CaO	A	< 1	2.13 *(2.06; 2.06; 2.74)*	2.09 *(2.46)*	2.84	2.47	2.17	2.34	2.48 *(2.58; 2.61; 2.49)*
Na_2O	A	< 1	0.32 *(nd; 0.24; 0.26)*	0.20 *(0.22)*	0.27	0.27	0.18	0.25	0.49 *(0.46; nd; 0.43)*
K_2O	A	< 1	0.02 *(nd; 0.04; 0.02)*	0.02 *(0.02)*	0.01	0.02	0.01	0.02	0.03 *(0.04; nd; 0.03)*
P_2O_5	A	< 1	0.24 *(0.18; nd; nd)*	0.23	0.22	0.25	0.25	0.24	0.25 *(0.24; 0.24; 0.24)*
Co	B	4.2	0.060 *(0.08; 0.06; 0.06)*	0.057 *(0.06)*	0.058	0.056	0.061	0.058	0.061 (0.06; 0.068; 0.066)
Ni	A	< 1	1.39 *(1.13; 1.20; nd)*	1.30	1.31	1.28	1.28	1.31	1.33 *(1.42; 1.39*; 1.42)*
S[7]	*C*	-	*2.1* *(nd; nd; nd)*	*0.7*	*0.5*	*0.5*	*0.9*	*0.94*	*2.1* (2.10; nd; 2.08)
Total			98.98	98.10	98.91	97.52	97.58	98.18	99.49

[1] Analytical method, laboratory: A: XRF, Institut für Geologie und Mineralogie, University of Cologne; B: ICP-MS, Institut für Mineralogie, University of Münster; C: SEM-EDX, Institut für Planetologie, University of Münster
[2] Reproducibilityof the measured values (in %, RSD)
[3] Literature data (Wolf and Palme, 2001; Weckwerth, 2014; Kallemeyn and Rubin, 1995) in parenthesis. nd: not determined
[4] Literature data (Kallemeyn and Rubin, 1995) in parenthesis
[5] Literature data (Jarosewich et al.,1987; Stracke et al., 2012, average of 39 samples; Braukmüller et al., 2018) in parenthesis.
* XRF/ICP-MS average.
[6] Mean of literature values; own value (0.72 wt.%) probably biased by unknown contamination
[7] Rough estimate; recalculated values relative to Allende (SEM-EDX; see section 3.2.1)

Table 10. Bulk chemical composition of the investigated samples (trace elements; ppm). Numbers in italics indicate values that show evidence for modification by terrestrial weathering. Sample abbreviations: see Table 8.

	Lab[1]	RSD[2] (%)	Clg[3]	Loo[4]	LoV	033	13400	Mean CL[5]	Allende	Allende (Literature)[6]		
										Stra	Brau	Others
Li	B	1.7	*2.10*	*2.13*	*2.07*	*2.10*	*1.97*		1.69			1.81[a]; 1.64[b]
Sc	D	4.9	15.5 (12.0; 9.4)	10.5 (11.2)	15.3	10.6	11.5	12.7	11.8			11.3[a]; 10.8[b]; 10.7[c]
V	B	2.2	85.6 (106; 91)	73.3 (102)	85.5	81.4	81.6	81.5	95.9	90.2*	92.6	95.2[a]; 91[b]; 91[c]
Zn	A	< 1	56.7 (60; 33)	33.7 (50)	32.5	43.5	51.6	43.6	102	106	123	119[a];118[d]
Se	D	32	5.05 (3.2; 3.2)	5.78 (3.3)	2.62	5.18	3.04	4.33	9.57			9.21[d]; 8.25[e]
Rb	B	2.3	0.29	0.92	0.42	0.50	0.18	0.46	1.21	1.32	1.15	1.18[a]; 1.17[b]
Sr	B	0.6	14.8	15.3	18.8	*24.2*	15.5	16.1	14.6	15.7		15.6[b];15.6[c]
Y	B	1.2	2.66	3.75	2.81	3.77	2.48	3.09	2.60	2.63		2.88[a]; 2.77[b]
Zr	B	0.7	6.82	8.89	7.40	9.15	6.20	7.69	6.60	6.77	6.45	6.61[a]; 7.1[b]
Nb	B	2.4	0.519	0.620	0.662	0.574	0.535	0.582	0.531	0.569	0.503	0.573[a]; 0.58[b]
Mo	B	0.2	1.52	1.50	1.64	1.40	1.57	1.53	1.51	1.45		1.64[e]; 1.44[f]
Te	D	8.6	0.781	0.575	0.528	0.588	0.611	0.617	1.21		1.04	0.94[e]; 0.944[g]
Cs	B	2.8	0.024	0.060	0.042	0.044	0.011	0.036	0.088	0.098	0.080	0.086[b]
Ba	B	0.3	*33.9*	*15.2*	*13.0*	*61.6*	*73.3*		4.49	4.74	4.21	4.53[a]; 4.6[b]; 4.7[e]
La	B	0.2	0.642 (0.505; 0.89)	*1.482*	0.527	*0.959*	0.461	0.543	0.487	0.490	0.471	0.516[a]; 0.498[b]
Ce	B	0.1	*1.400*	*3.114*	*1.318*	*2.148*	*1.152*		1.24	1.24	1.21	1.29[a]; 1.29[b]
Pr	B	0.6	0.228	*0.459*	0.201	*0.316*	0.179	0.203	0.193	0.192	0.191	0.201[a]; 0.195[b]
Nd	B	0.4	1.116	*2.006*	1.006	*1.515*	0.891	1.004	0.975	0.967	0.998	1.02[a]; 0.989[b]
Sm	B	0.2	0.335 (0.311; 0.34)	*0.506*	0.324	*0.427*	0.283	0.314	0.316	0.313	0.328	0.329[a]; 0.310[b]; 0.331[e]
Eu	B	0.4	0.115 (0.118; 0.12)	*0.153*	0.117	*0.139*	0.109	0.114	0.111	0.115	0.110	0.114[a]; 0.108[b]
Gd	B	0.1	0.404	*0.596*	0.407	*0.530*	0.364	0.392	0.397	0.401	0.439	0.417[a]; 0.409[b]
Tb	B	0.2	0.074	*0.102*	0.074	*0.091*	0.067	0.072	0.073	0.072	0.074	0.076[a]; 0.073[b]
Dy	B	0.4	0.482	*0.661*	0.496	*0.582*	0.441	0.473	0.479	0.479	0.499	0.508[a]; 0.483[b]
Ho	B	0.1	0.107	*0.150*	0.110	*0.133*	0.098	0.105	0.104	0.100		0.107[a]; 0.103[b]
Er	B	0.4	0.309	*0.432*	0.318	*0.403*	0.287	0.305	0.300	0.299	0.304	0.310[a]; 0.305[b]
Tm	B	0.8	0.054	0.057	0.053	0.057	0.048	0.054	0.054	0.053	0.053	0.056[a]; 0.050[b]
Yb	B	0.1	0.317 (0.329; 0.3)	0.360 (0.338)	0.343	0.345	0.305	0.334	0.326	0.319	0.327	0.325[a]; 0.302[b]
Lu	B	1.8	0.046 (0.052; 0.04)	*0.062*	0.048	*0.061*	0.043	0.046	0.044	0.046	0.047	0.046[a]; 0.046[b]
Hf	B	2.6	0.203 (nd; 0.25)	0.264	0.206	0.262	0.178	0.223	0.192	0.188	0.191	0.202[a]; 0.199[b]
Ta	B	0.1	0.030	0.037	0.032	0.032	0.028	0.032	0.033	0.033		0.034[a]; 0.041[b]
Tl	B	10	0.004	*0.022*	0.006	*0.064*	0.007	0.006	0.071		0.062	0.059[e]
Pb	B	0.6	0.325	0.635	0.196	0.508	0.183	0.369	1.29	1.52	1.08	1.27[a]; 1.25[b]
Th	B	3.9	*0.080*	*0.315*	*0.076*	*0.106*	*0.072*		0.084	0.078	0.056	0.059[a]; 0.082[b]
U	B	4.1	*0.037*	*0.041*	*0.028*	*0.100*	*0.031*		0.015	0.017	0.013	0.015[a]; 0.018[b]

[1] Analytical method and laboratory: A: XRF, Institut für Geologie und Mineralogie, University of Cologne; B: ICP-MS, Institut für Mineralogie, University of Münster, Germany; D: LA-ICP-MS, Institut für Mineralogie, University of Münster.

[2] Reproducibility of the measured values (in %, RSD)

[3] Literature data (Kallemeyn and Rubin, 1995; Weckwerth, 2014) in parenthesis; nd: not determined

[4] Literature data (Kallemeyn and Rubin, 1995) in parenthesis

[5] Numbers in italics (individual meteorite data) have been excluded from mean value calculation

[6] Literature data for Allende. Averaged values are shown in Figs. 9-10. Stra: Stracke et al. (2012; average of 39 subsamples; * XRF/ICP-MS average). Brau: Braukmüller et al. (2018; Smithsonian standard). Others: [a] Barrat et al. (2012); [b] Pourkhorsandi et al. (2017b); [c] Greenwood et al. (2010); [d] Hezel and Palme (2008); [e] Wang et al. (2014); [f] Burkhardt et al. (2014); [g] Hellmann et al. (2020).

1406 **Table 11.** Bulk O isotopic composition of the investigated CL chondrites.

	Coolidge	Loongana 001	LoV 051	NWA 033	NWA 13400
$\delta^{17}O \pm 1\sigma$ (‰)*	-6.835 ± 0.216	-4.781 ± 0.170	-7.626 ± 0.486	-3.911 ± 0.164	-4.017 ± 0.023
$\delta^{18}O \pm 1\sigma$ (‰)*	-3.336 ± 0.169	-1.035 ± 0.136	-4.151 ± 0.518	0.102 ± 0.228	-0.021 ± 0.007
$\Delta^{17}O \pm 1\sigma$ (‰)*	-5.101 ± 0.128	-4.243 ±0.099	-5.467 ± 0.216	-3.964 ± 0.046	-4.006 ± 0.026

1407 * Mean of 2 measurements, each. ±: 1 standard deviation

1408

1409 **Table 12**. Bulk Ti and Cr isotopic composition of the investigated CL chondrites and Allende.

	N [Ti]	$\varepsilon^{46}Ti \pm 2\sigma$	$\varepsilon^{48}Ti \pm 2\sigma$	$\varepsilon^{50}Ti \pm 2\sigma$	N [Cr]	$\varepsilon^{53}Cr \pm 2\sigma$	$\varepsilon^{54}Cr \pm 2\sigma$
Coolidge	10	0.50 ± 0.09	0.07 ± 0.10	2.63 ± 0.10	8	0.07 ± 0.08	0.81 ± 0.10
Loongana 001	10	0.43 ± 0.13	–0.07 ± 0.07	2.57 ± 0.09	11	0.06 ± 0.08	0.68 ± 0.18
LoV 051	10	0.52 ± 0.06	–0.05 ± 0.04	2.85 ± 0.08	8	0.05 ± 0.07	0.76 ± 0.12
NWA 033	10	0.44 ± 0.10	–0.08 ± 0.09	2.35 ± 0.05	12	0.05 ± 0.11	0.64 ± 0.12
NWA 13400	10	0.53 ± 0.06	–0.05 ± 0.03	2.60 ± 0.07	9	0.14 ± 0.13	0.70 ± 0.13
Average CL		0.48 ± 0.04	–0.03 ± 0.03	2.60 ± 0.05		0.07 ± 0.04	0.71 ± 0.06
Allende	12	0.70 ± 0.06	–0.06 ± 0.04	3.21 ± 0.11	6*	0.12 ± 0.12*	0.96 ± 0.22*
					4*	0.11 ± 0.10*	1.06 ± 0.30*

1410 All reported uncertainties are Student-t 95% confidence intervals (95% CI). N: Number of analyses of the same solution.

1411 * Schneider et al. (2020)

FIGURE CAPTIONS

Fig. 1. Overall texture and lithologic components of the Loongana 001 meteorite as an example for the proposed CL group of carbonaceous chondrites (a: back-scatter electron image; b: phase map including color coding). Beside the omnipresent metal-rich porphyritic Type-I chondrules (PO, POP) with irregular shapes (1,6), the following components are visible: 2) Barred olivine (BO) chondrule; 3) Al-rich chondrule; 4) Chondrule fragment; 5) Irregularly shaped chondrule adhering to a larger one; 6) Chondrule with thick pyroxene rim (7) and olivine-rich core; 8) Ca-Al-rich inclusion (CAI).

Fig. 2. Frequency distributions of fayalite (Fa) values (a) and ferrosilite (Fs) values (b) in olivine and low-Ca pyroxene, respectively, in CL chondrites. Coolidge, Loongana, and NWA 033 show narrow Fa distributions. The samples LoV 051 and NWA 13400 show broader distributions, indicating a less intensive metamorphic overprint. The number of analyzed olivine and pyroxene grains are listed in Tables 4 and 5, respectively.

Fig. 3. Chondrule textures in CL chondrites. a) Typical porphyritic olivine-pyroxene (POP) chondrule with irregular and lobate outline (Coolidge). b) Chondrule with several protuberances in NWA 13400. c) Assortment of differently sized and irregularly shaped chondrules or melt shreds (NWA 13400). d) Complex chondrule (white outline), consisting of a porphyritic olivine (PO) chondrule core with irregular layers of adhering smaller chondrules or melt shreds, stacked on top of each other. The central chondrule is separated from these layers by an Fe-Ni layer (white). e) Layered olivine chondrule with concentric inner Fe-Ni layer and thin pyroxene rim (LoV 051). f) Multi-layered olivine chondrule with two cocentric inner Fe-Ni layers and an outer Fe-Ni layer (NWA 13400). g) Al-rich chondrule with fine-grained quench texture and large Al-rich enstatite crystals (dark gray; Loongana). h) Barred olivine (BO) chondrule of Type-II with igneous rim in NWA 13400. SEM-BSE images; dark gray: low-Ca pyroxene; medium gray: olivine; white to light gray: Fe-Ni metal, sulfides. White to light gray linear features are terrestrial oxidation products along cracks (SEM-BSE images).

Fig. 4. Opaque phases in CL chondrites. a) Polycrystalline kamacite grain in a Coolidge chondrule, showing taenite exsolutions (light gray) and exsolutions of chromite and merrilite (black dots) along kamacite grain boundaries; b) Rare side-by-side occurrence of isolated kamacite (right center) and taenite grains (left center) in a chondrule in NWA 033; other grains are FeS; c) Intergrowth texture of sulfide (FeS; gray) and kamacite (white) in a LoV chondrule; d) Very large polycrystalline FeS grain in a Coolidge chondrule; white: kamacite. (SEM-BSE images).

Fig. 5. Frequency distributions of apparent chondrule sizes (100 µm binning), measured on BSE photomosaics. a) Frequency distributions in the investigated CL chondrites; b) Average distribution in CL chondrites (blue solid line, calculated from data in a). Frequency distributions for the CV chondrites Allende (CV_{oxA}, red dashed line) and the CR chondrite NWA 7020 (black dotted line), obtained in this study, are shown for comparison. Please note the different scaling of the size axes in a) and b). n: number of measured chondrules.

Fig. 6. Textures and components of refractory inclusions in CL chondrites. a) Complex CAI in Loongana, consisting of fine-grained subunits (anorthite, spinel) which are rimmed by Ca-rich pyroxene (medium gray), and some FeS (white); b) CAI in NWA 13400, mainly consisting of subhedral-euhedral spinel (medium-dark gray), FeS (white), partly surrounded by a spinel rim; c) CAI in Coolidge, rimmed by a spinel and diopside layer, probably a former Wark-Lovering rim. This inclusion contains a mineral assemblage consisting of FeS, TiO_2, and spinel, embedded in extremely fine-grained groundmass; d) Cl-apatite in a CAI in NWA 13400 (left center, light gray); e) Refractory metal nugget (light gray to white; rich in Os, Ir, Pt, Ru) in a CAI in Loongana; f) Amoeboid olivine aggregate (AOA) in LoV, intermingled with CAI material (right part of the inclusion). White to light-gray linear features in the images are terrestrial oxidation products along cracks (SEM-BSE images).

Fig. 7. Matrix in CL chondrites. a) Overview of Loongana matrix, showing chondrule and mineral fragments (mostly olivine and low-Ca pyroxene), embedded in a fine-grained groundmass of very small grains of olivine and low-Ca pyroxene, with interstitial oxidation products of metals and sulfides. Microtextures of Matrix are shown for the CL chondrites Loongana (b), Coolidge (c), LoV 051 (d), NWA 033 (e), and NWA 13400 (f). The size distributions are bimodal with a coarser-grained fragment population, cemented by a finer-grained groundmass. The latter possibly crystallized during thermal metamorphism. Black to medium gray: silicates (olivine and pyroxene); light gray to white: oxidation products of metals and sulfides (SEM-BSE images).

Fig. 8. Bulk chemical compositions of CL chondrites (red filled circles; encircled in b) to d)) and other groups of carbonaceous (CI, CM, CO, CV, CR, CK4) and non-carbonaceous chondrites (literature data). a) Ratios of lithophile elements (Si/Mg vs. Al/Mg), revealing data cluster for carbonaceous chondrites, ordinary chondrites + R chondrites, and separate values for EL and EH chondrites (data from Hutchison, 2004; his table 2.1). The CL data plot within the field of the other carbonaceous chondrite groups. b) Al_2O_3 vs. MnO concentrations; the volatile lithophile element Mn is considerably depleted in CL chondrites compared to the other groups; the Al_2O_3 concentrations are in the range of CV and CK chondrites. c) Al_2O_3 vs. Zn concentrations; the CL chondrites show, on average, the lowest Zn concentrations among all carbonaceous chondrite groups. d) Zr vs. Rb concentrations; CL chondrites show a characteristic combination of low Rb and high Zr concentrations. Literature data for b) to d): CI (Lodders et al., 2009); Others (mean values, where possible): Kallemeyn and Wasson (1981, 1982); Jarosewich et al. (1987); Kallemeyn et al. (1991, 1994); Wolf and Palme (2001); Jarosewich (2006); Greenwood et al. (2010); Braukmüller et al. (2018).

Fig. 9. CI-normalized (Lodders et al, 2009) lithophile element concentrations in CL chondrites and other carbonaceous chondrite groups. Elements are arranged in the order of increasing volatility (Wood et al. 2019). a) Data for CL chondrites (colored curves, circles) and Allende (black curve, squares), together with Allende literature data (dashed curve; see Tables 9-10). The volatile lithophile elements Mn, Na, K, Rb, and Cs are moderately to strongly depleted compared to Allende. b) Mean concentrations in the CL chondrites (red solid curve, filled circles) and other carbonaceous chondrite

groups (CM, CO, CV, CR, CK4; literature values; black curves). The CL-trend of volatile element depletion and enrichment of other elements is evident. Literature data (mean values, where possible): Knab (1981); Kallemeyn and Wasson (1981); Jarosewich et al. (1987); Kallemeyn et al. (1991, 1994); Wolf and Palme (2001); Jarosewich (2006); Greenwood et al. (2010); McCoy-West et al. (2017); Braukmüller et al. (2018).

Fig. 10. CI-normalized (Lodders et al., 2009) concentrations of siderophile and chalcophile elements in CL chondrites and other carbonaceous chondrite groups. Elements are arranged in the order of increasing volatility (Wood et al. 2019). a) Data for CL chondrites (colored curves, circles) and Allende (black curve, squares), together with Allende literature data (dashed curve; see Tables 9-10). b) Mean concentrations in the CL chondrites (red curve, filled circles) and other carbonaceous chondrite groups (CM, CO, CV, CR, CK4; literature values; black curves). The concentrations of siderophile elements in CL chondrites are in the range of those in the other groups, with the highest value for the most refractory element (Mo). The concentrations of chalcophile elements in CL chondrites are the lowest of all other groups. Literature data (mean values, where possible): Matza and Lipschutz (1977; Tl in the Karoonda CK chondrite); Kallemeyn and Wasson (1981); Palme and Rammensee (1981); Jarosewich et al. (1987); Bischoff et al. (1993; Mo in the Acfer 059/El Djouf 001 CR chondrite); Kallemeyn et al. (1991, 1994); Wolf and Palme (2001); Jarosewich (2006); Greenwood et al. (2010); Burkhardt et al. (2014; Mo in the Karoonda CK chondrite); Braukmüller et al. (2018).

Fig. 11. Bulk oxygen isotopic compositions of CL chondrites (red squares). Data fields for CO3 (Alexander et al., 2018), CV3 and CK (Greenwood et al., 2010), and CR chondrites (Schrader et al., 2011, 2014) are shown for comparison. All samples plot on or slightly to the side of the Carbonaceous Chondrite Anhydrous Mineral (CCAM) line (Clayton and Mayeda, 1999). Other reference lines: Primitive Chondrule Minerals line (PCM) (Ushikubo et al., 2011); Young and Russell line (Y&R) (Young and Russell, 1998) , Terrestrial Fractionation Line (TFL) are shown for comparison. Three of the samples plot within the fields of CV3 and CK chondrites, together with Allende (this study). The meteorites Coolidge and LoV 051 plot outside these fields and are characterized by a lower concentration of ^{17}O and ^{18}O.

Fig. 12. Bulk isotopic compositions of CL chondrites (filled circles; red). a) $\epsilon^{54}Cr$ vs. $\Delta^{17}O$; b) $\epsilon^{54}Cr$ vs. $\epsilon^{50}Ti$. Mean values for other chondrite groups are shown for comparison (open diamonds: carbonaceous chondrites; open circles and squares: non-carbonaceous chondrites). All carbonaceous chondrites (including CL chondrites) exhibit negative Δ17O values and coupled ε50Ti–ε54Cr excesses. The data for CL chondrites form a tight cluster at a unique position in the ε54Cr-ε50Ti diagram, indicating their distinctness to the other groups. All reported uncertainties are Student-t 95% confidence intervals (95% CI). The chondrite groups are shown as composite points averaging multiple samples within each group. Literature data for Cr and Ti isotopes: Burkhardt et al. (2019); Mougel et al. (2018); Sanborn et al. (2019). Literature data for O isotopes: Clayton and Mayeda (1999), Dauphas and Schauble (2016), Burkhardt et al. (2017).

1536 **Fig. 13.** Correlations between mean matrix abundances (mass fraction) and mean $\epsilon^{54}Cr$ values (a)
1537 and mean concentrations of selected volatile elements (b-d), respectively, in the various carbonaceous
1538 chondrite groups. a) The mean CL value plots at the lower end of the chondrule-matrix mixing line,
1539 indicating that the low $\epsilon^{54}Cr$ value of CL chondrites reflects the low matrix abundance of this group.
1540 The intersection of the mixing line with the ordinate reveals the mean $\epsilon^{54}Cr$ values for CV, CO, and
1541 CM chondrules (Hellmann et al., 2020), as well as for CL chondrules. CR chondrites are exceptional;
1542 for details see Hellmann et al. (2020). b-d) The mean CL values plot at the lower end of the
1543 correlations, indicating that the low concentration of the volatile elements Zn, Se, and Te reflect the
1544 low matrix abundance of the CL group, as well. Data for the CI, CM, CV, CO, CR groups and Tagish
1545 Lake (TL) are from Hellmann et al. (2020).
1546

FIGURES

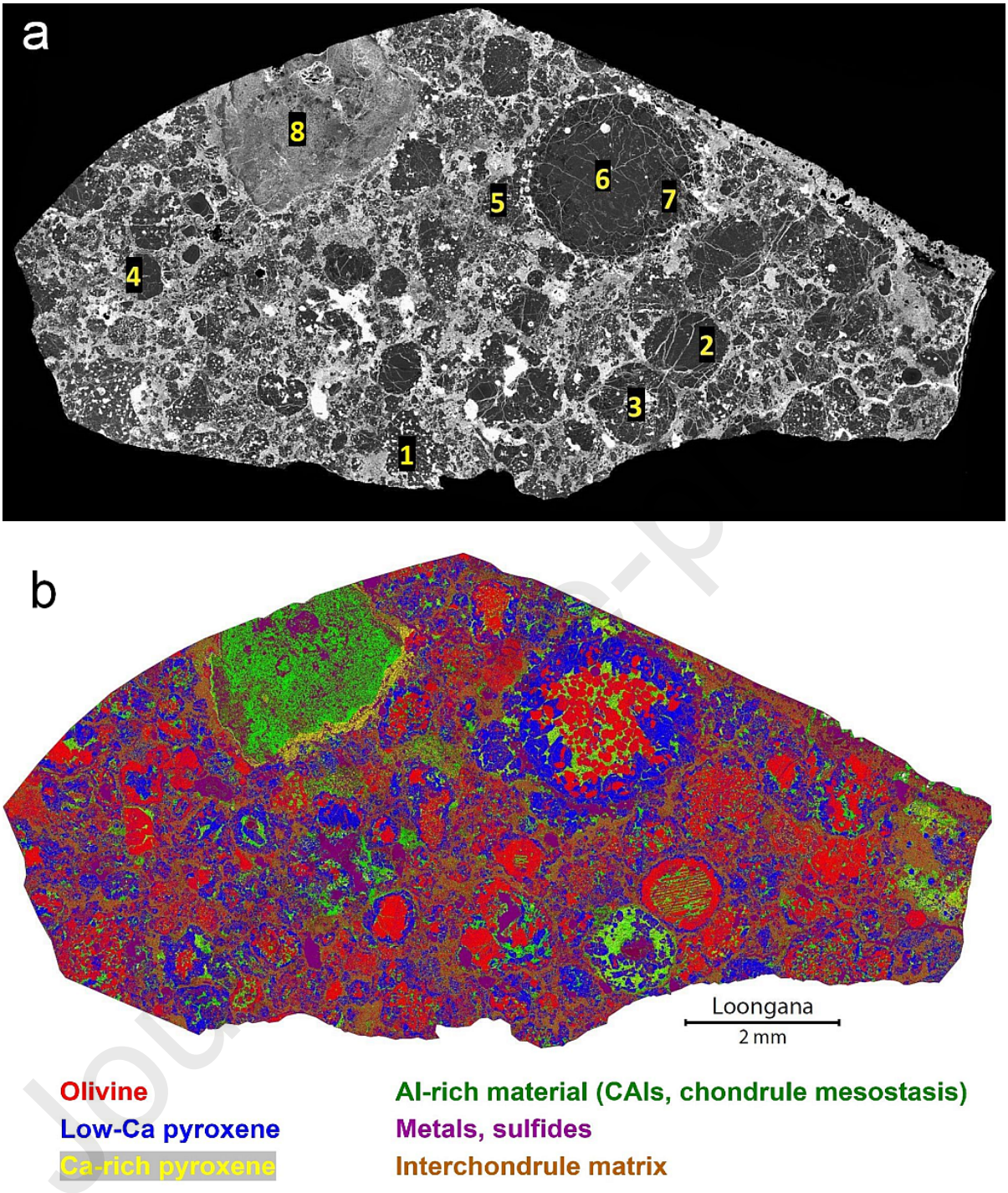

Fig. 1

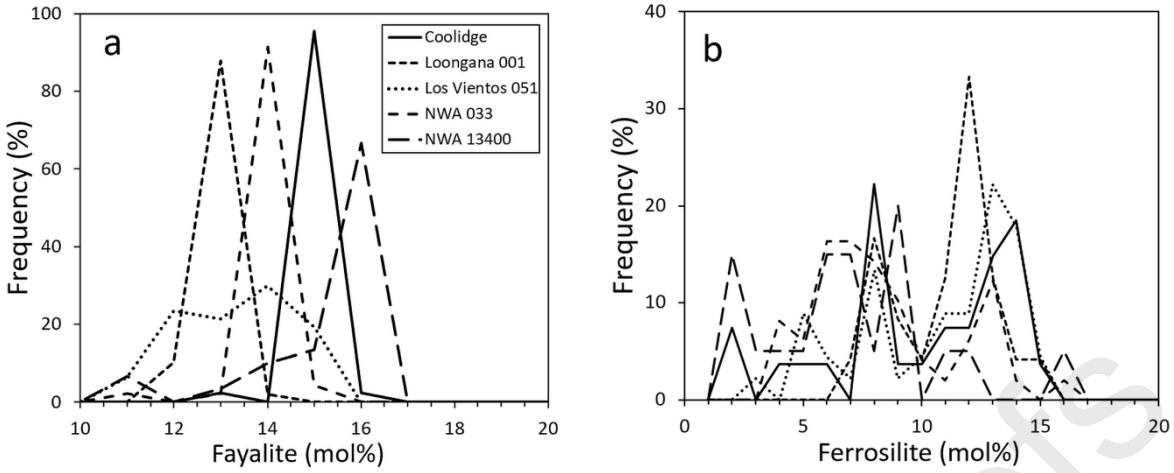

Fig. 2

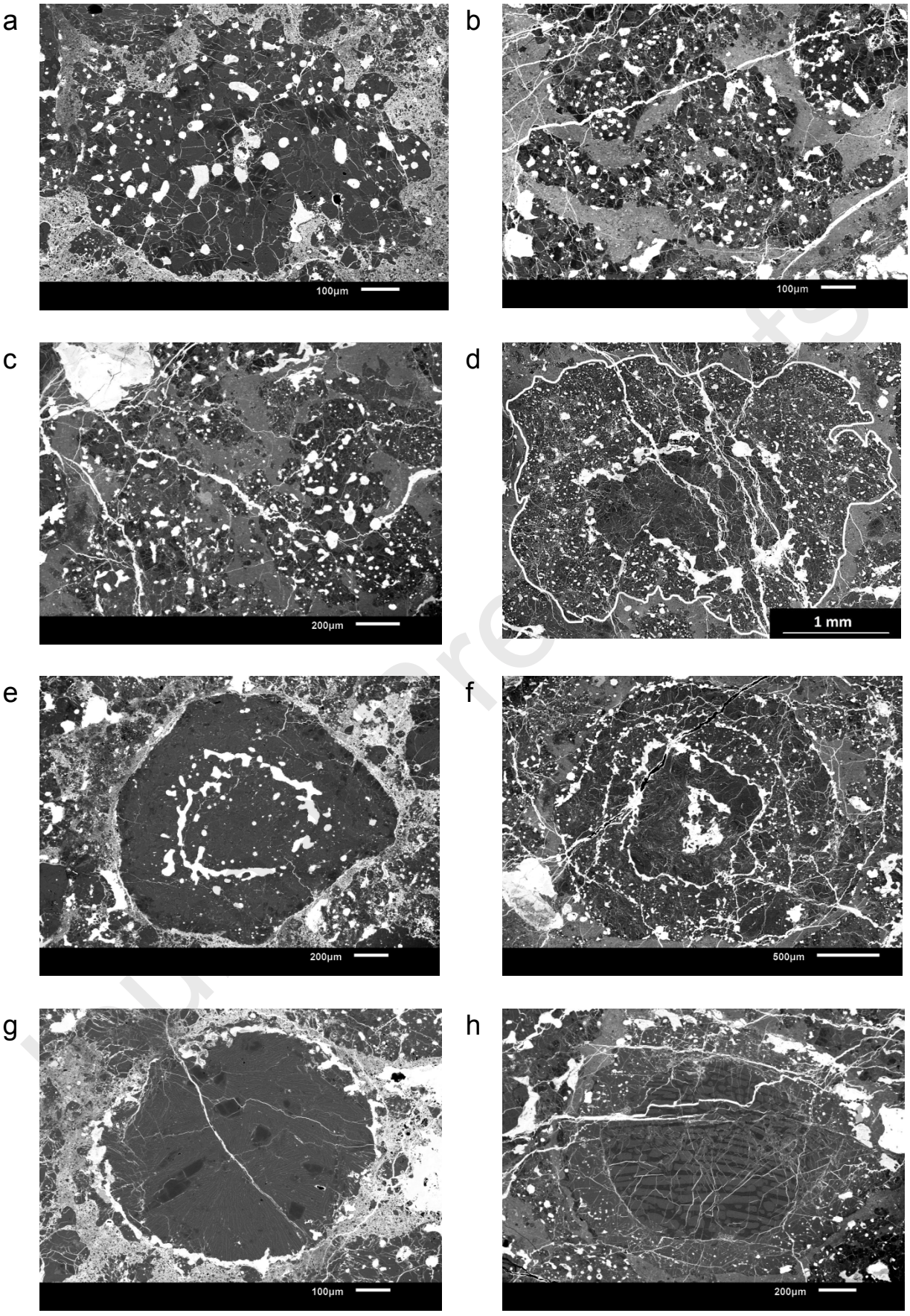

Fig. 3

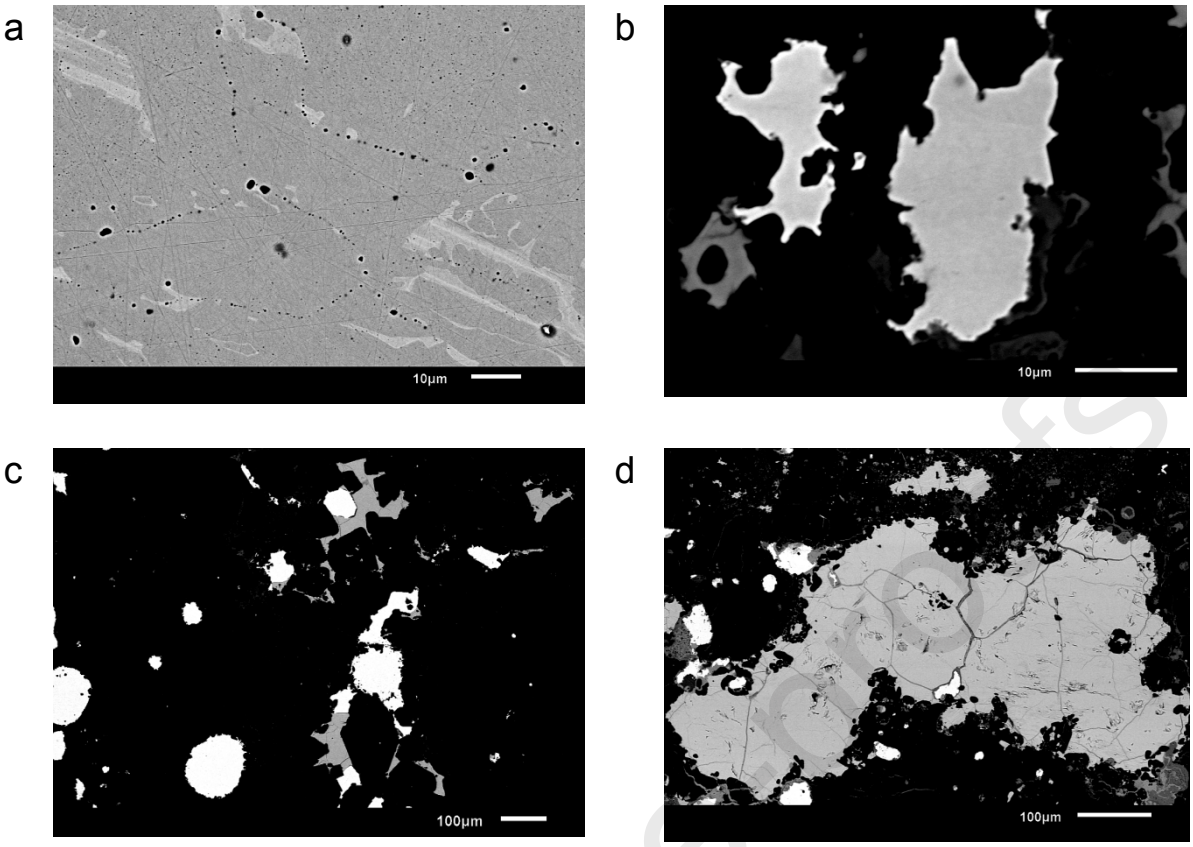

Fig. 4

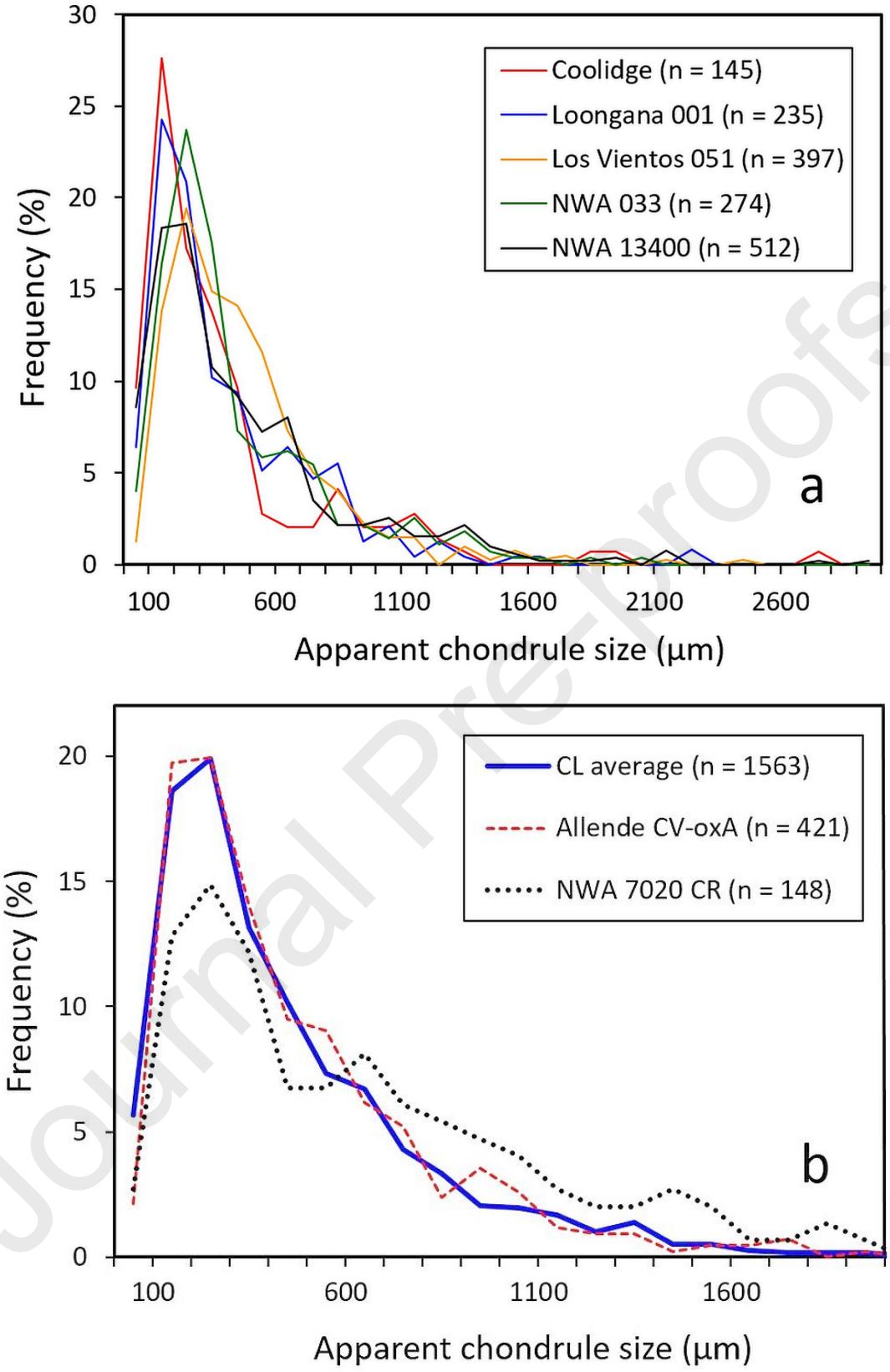

Fig. 5

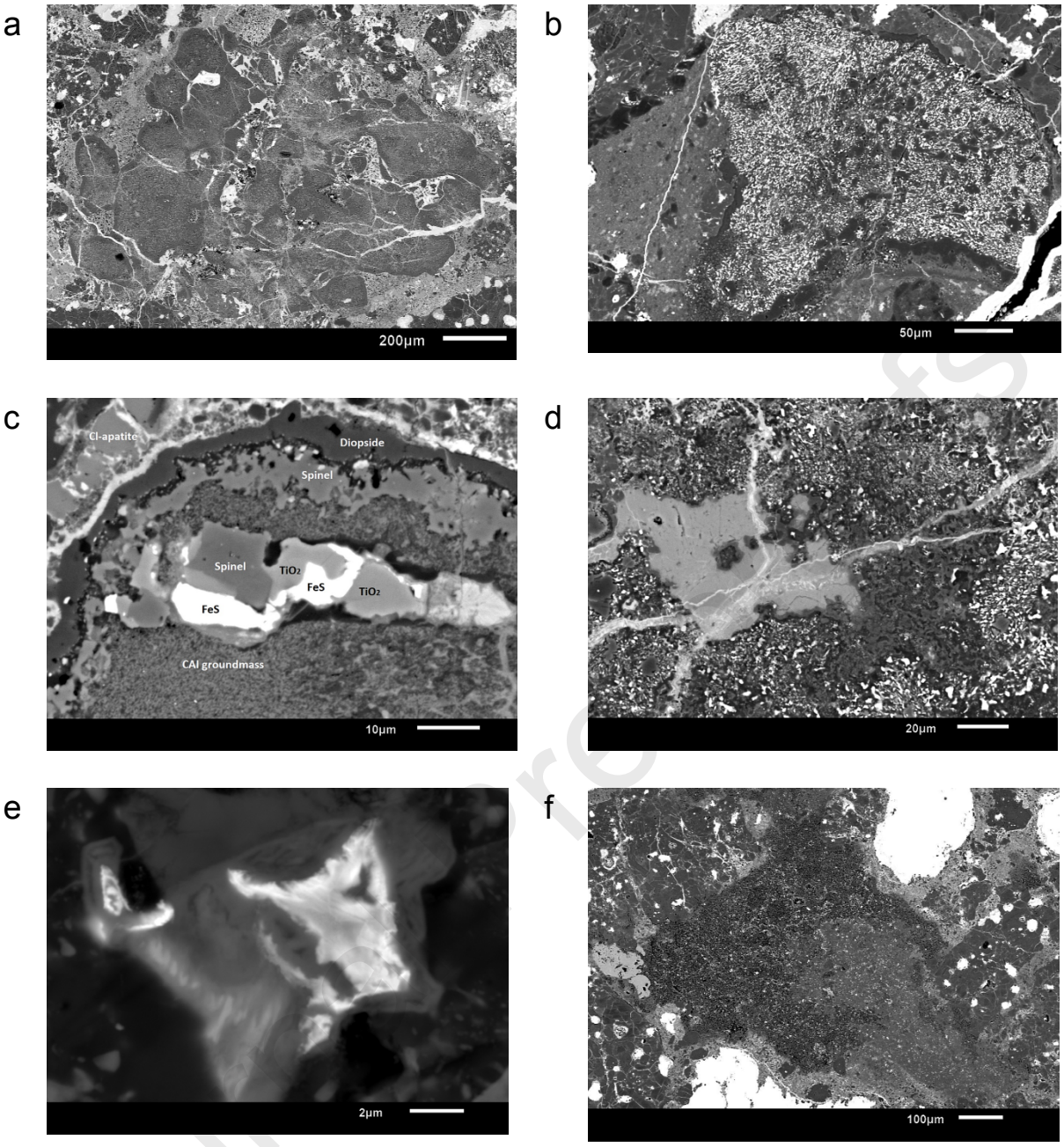
a
200µm
b
50µm
c
Cl-apatite
Diopside
Spinel
Spinel
TiO2
FeS
TiO2
FeS
CAI groundmass
10µm
d
20µm
e
2µm
f
100µm

Fig. 6.

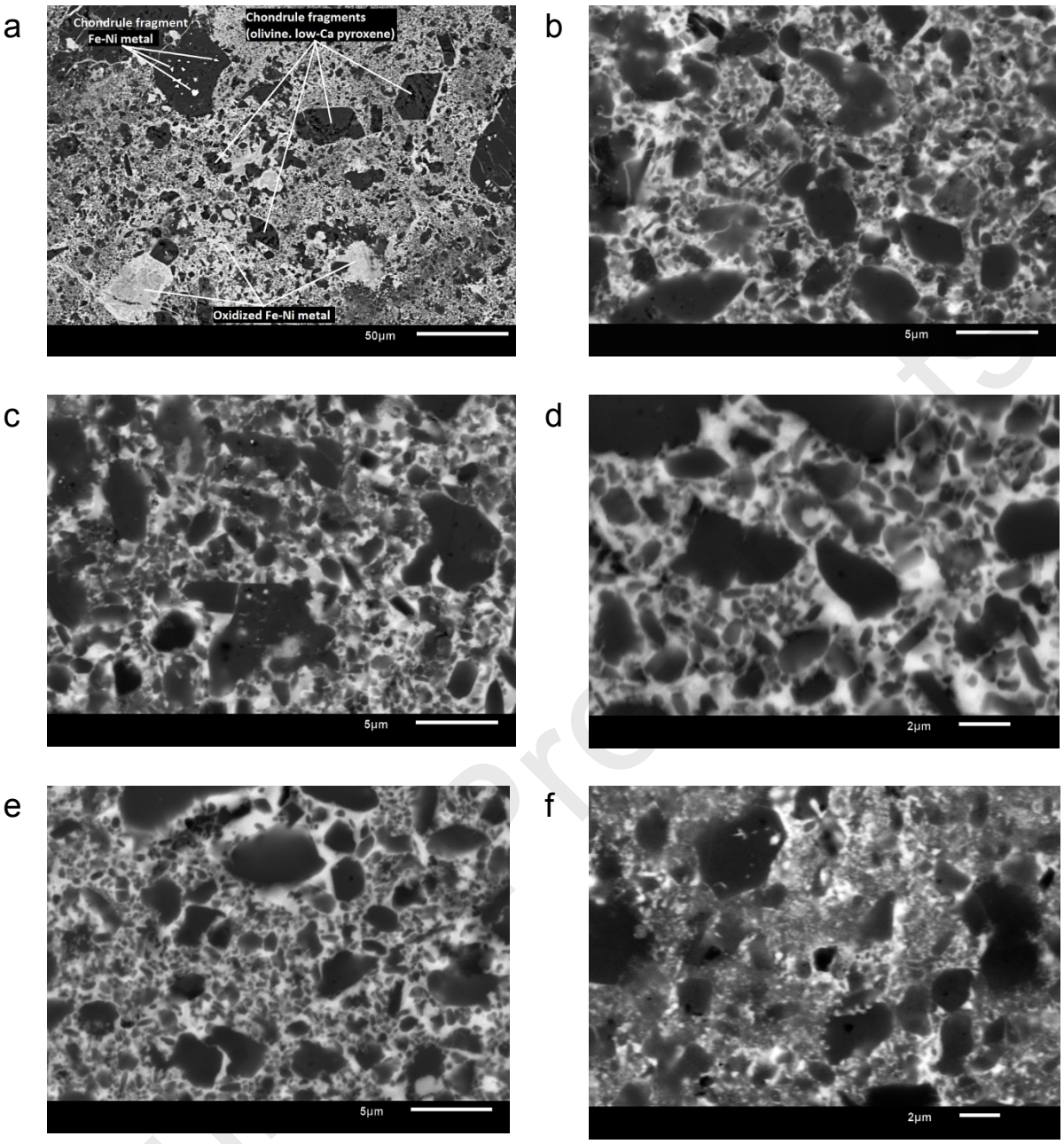
a
Chondrule fragment
Fe-Ni metal
Chondrule fragments
(olivine. low-Ca pyroxene)
Oxidized Fe-Ni metal
50μm
b
5μm
c
5μm
d
2μm
e
5μm
f
2μm

Fig. 7

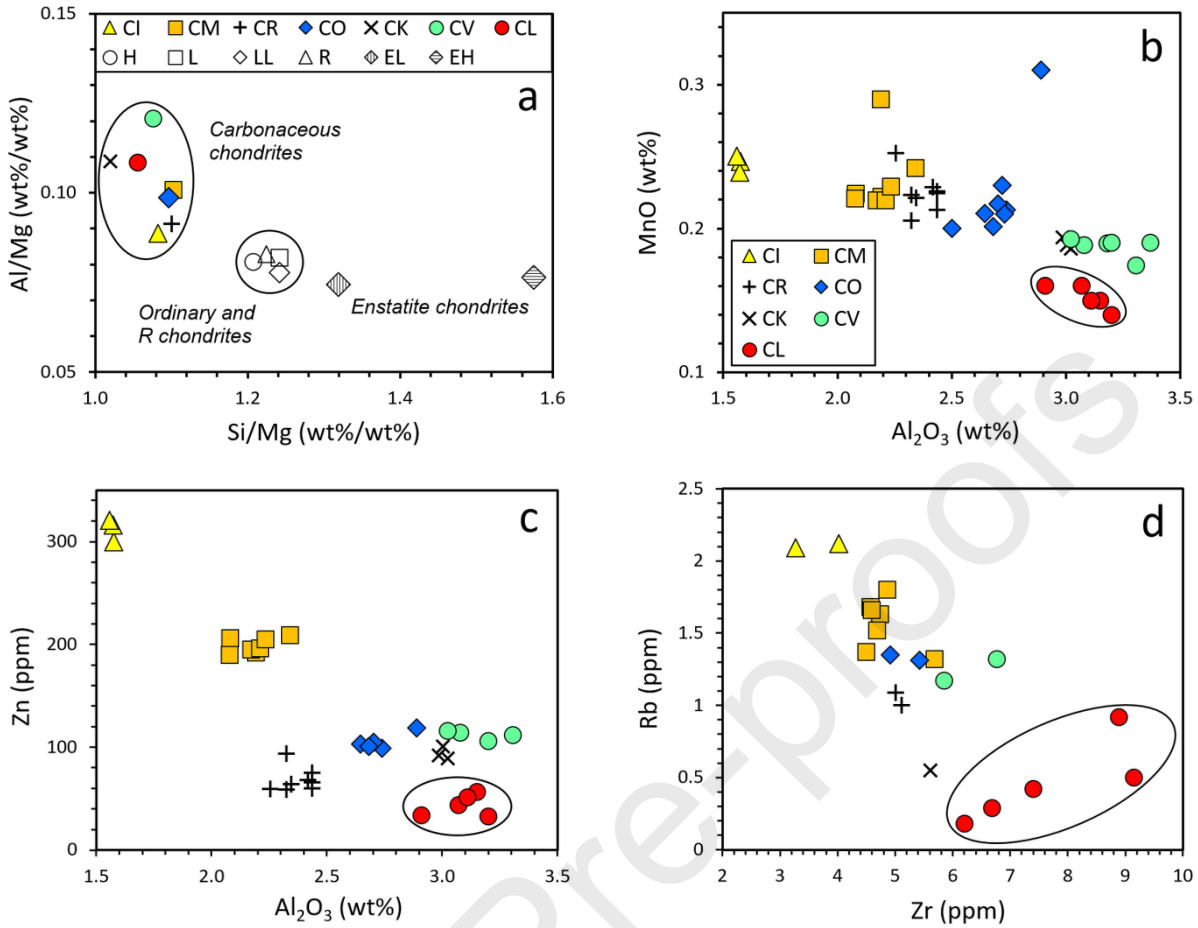

Fig. 8

1547

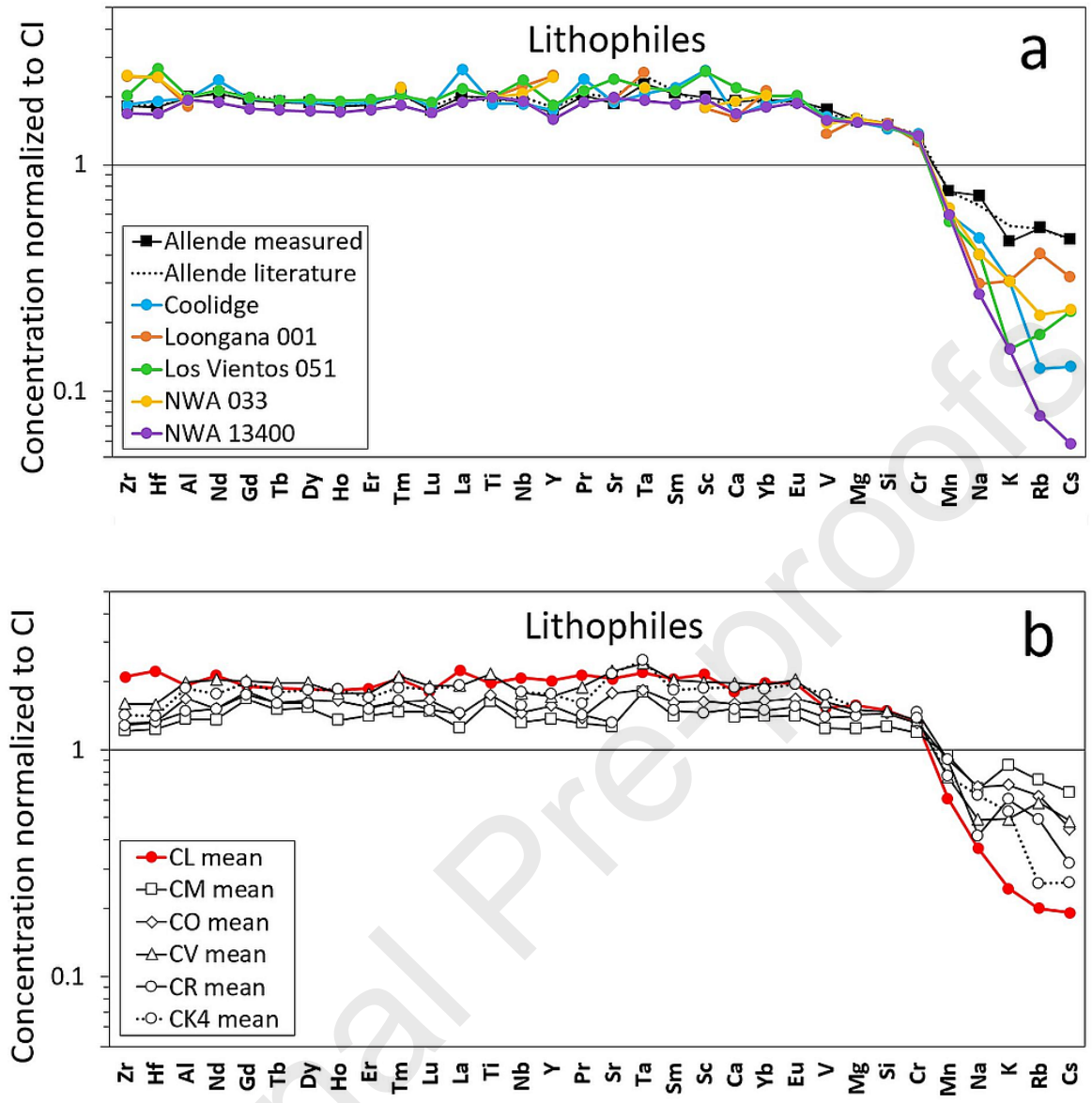

Fig. 9

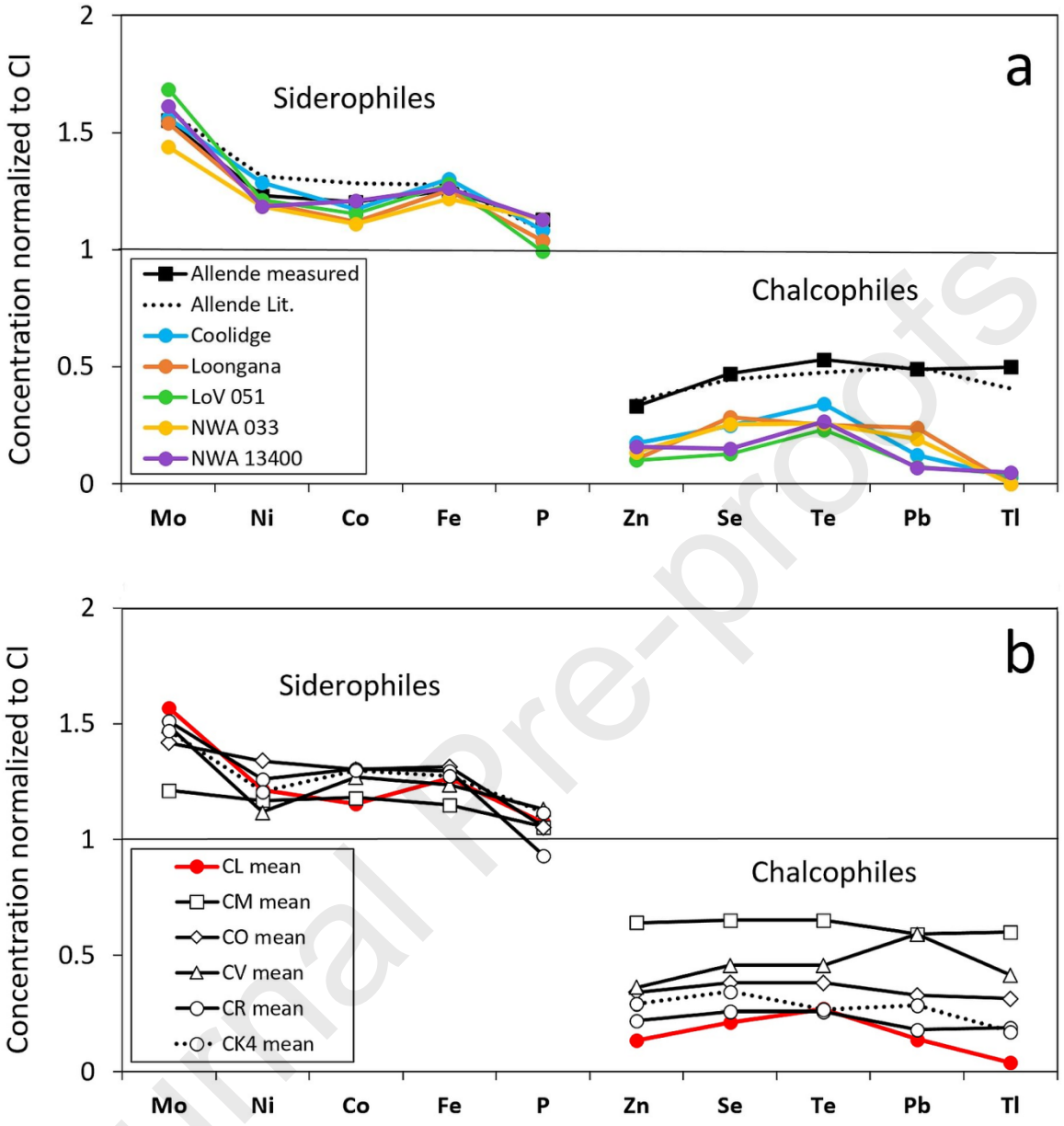

Fig. 10

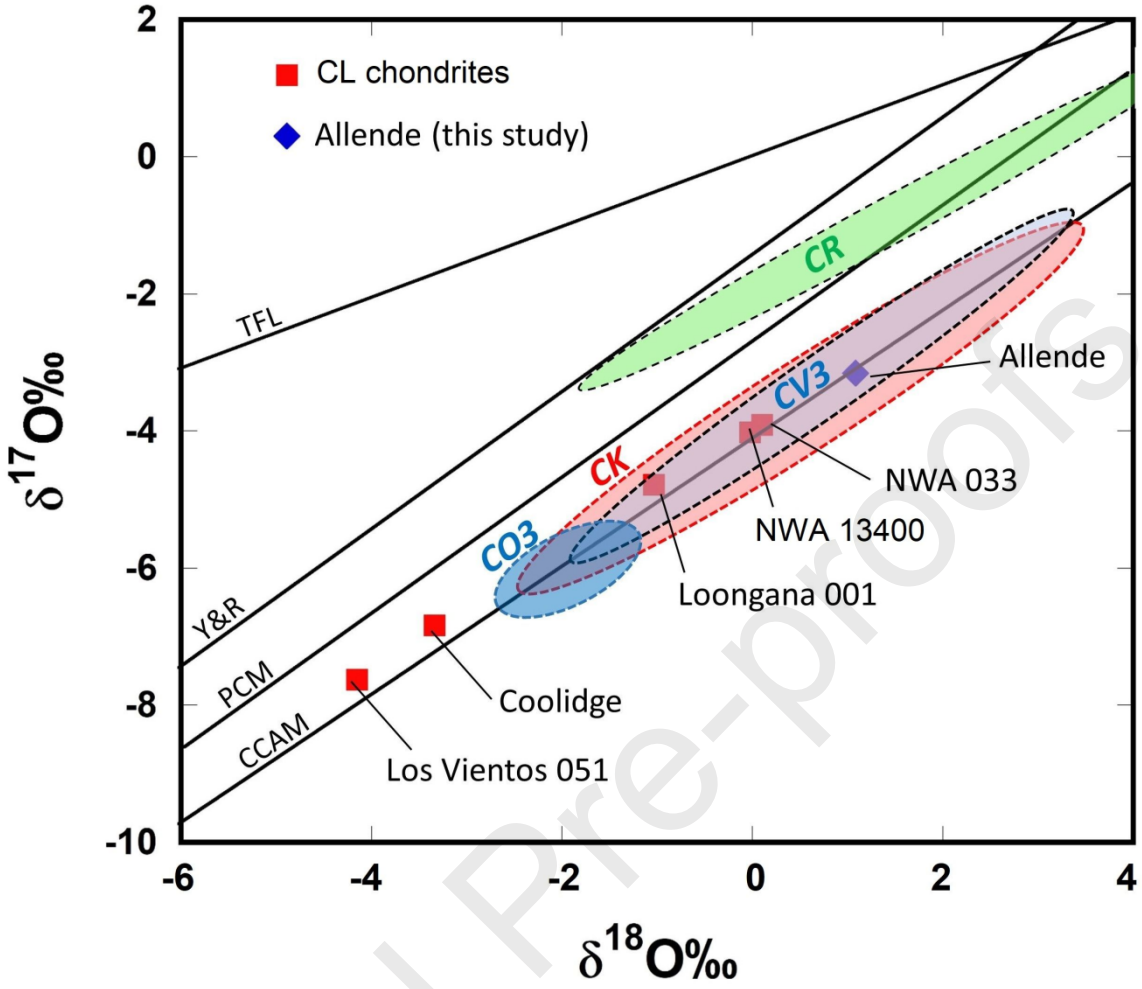

Fig. 11

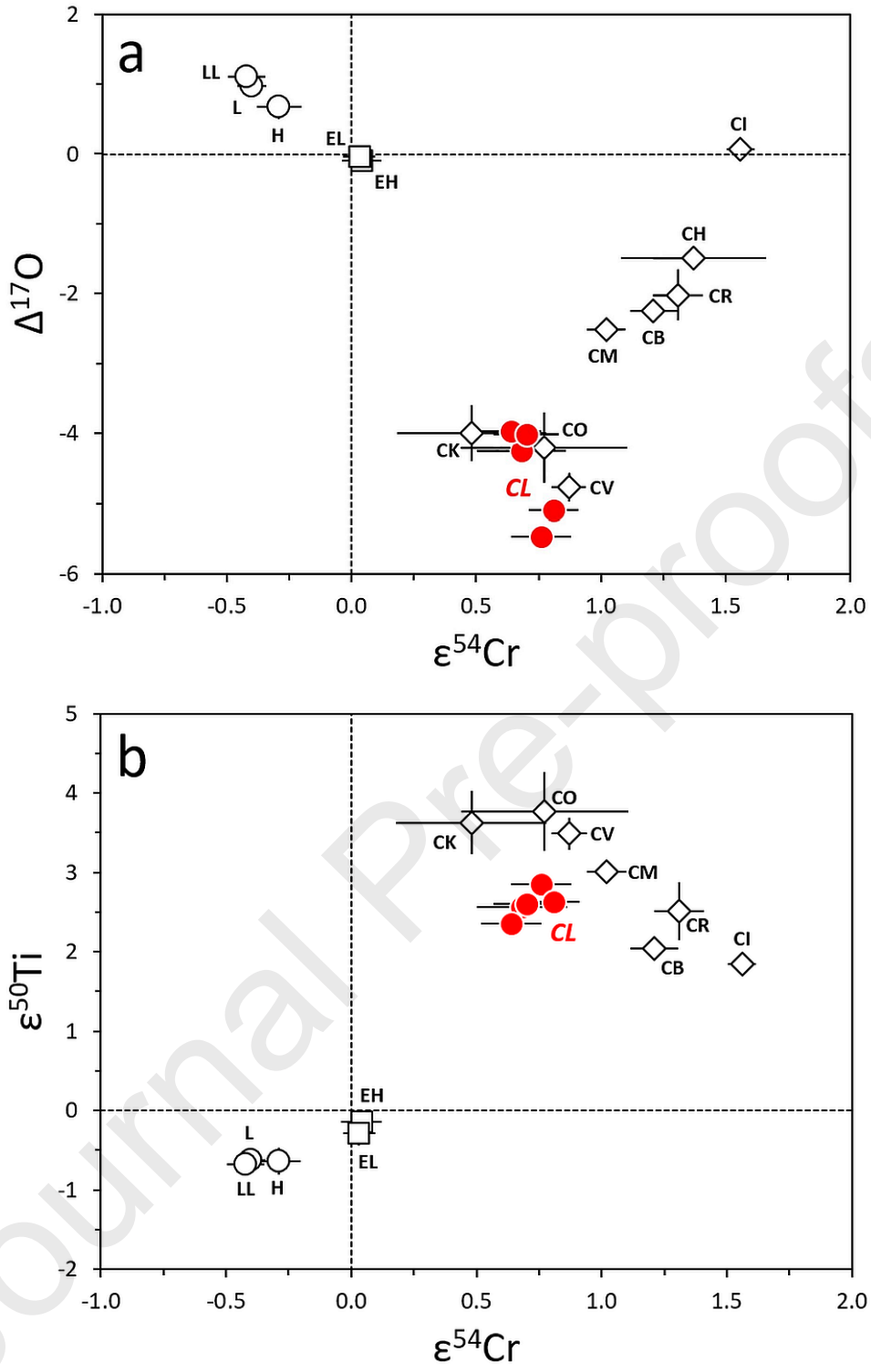

Fig. 12

1548

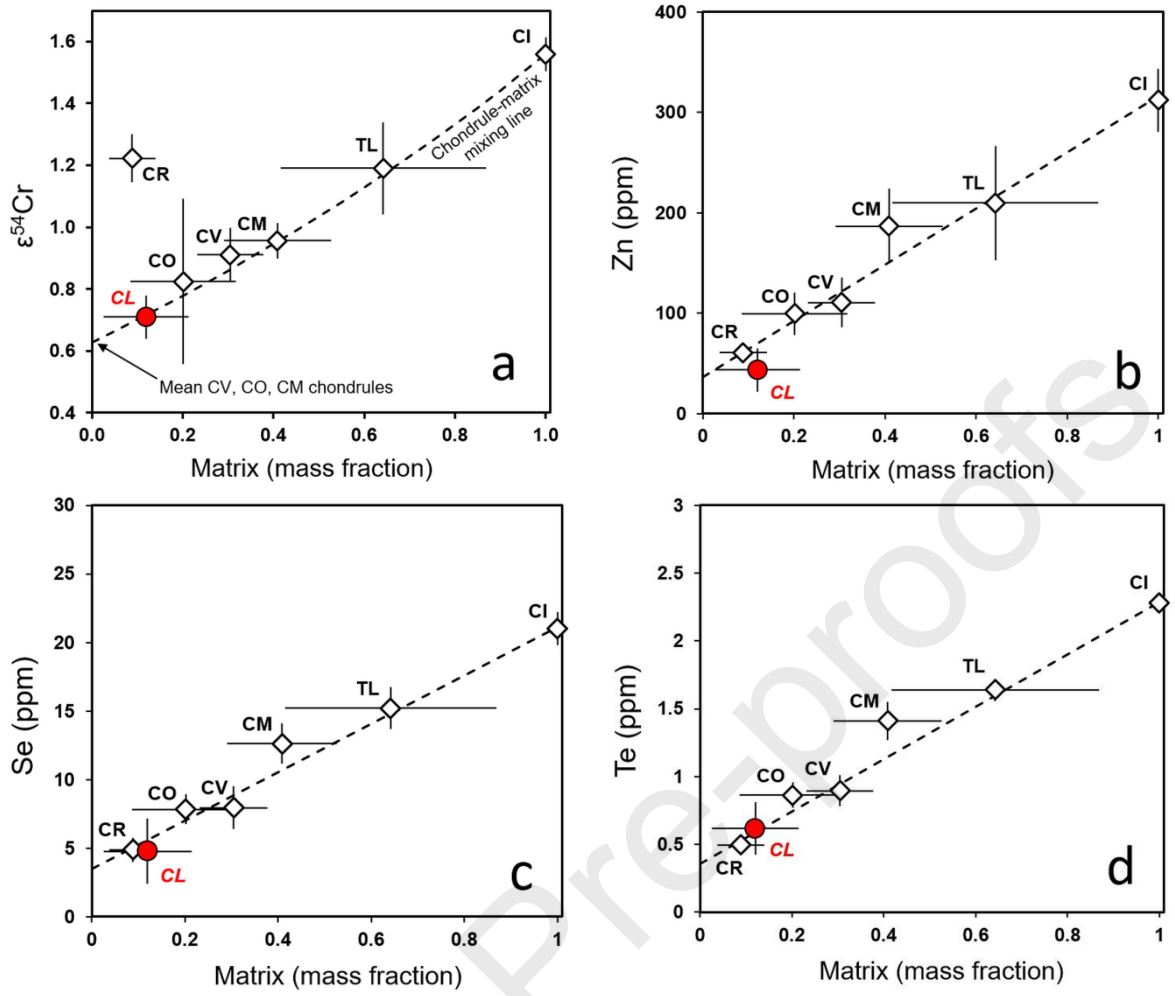

Fig. 13

1549

1550 • Five related meteorites define the Loongana (CL) group of carbonaceous chondrites
1551 • Coolidge, Loongana 001, LoV 051, NWA 033, and NWA 13400 represent CL
1552 chondrites
1553 • Strongest depletions of volatile elements in the CL group of carbonaceous chondrites
1554 • Unique positions of carbonaceous chondrites of the CL group in a $\varepsilon^{54}Cr$- $\varepsilon^{50}Ti$ diagram
1555 • Enrichment of ^{16}O in some CL chondrites compared to CO, CV, and CK chondrites
1556

Declaration of interests

☒ The authors declare that they have no known competing financial interests or personal relationships that could have appeared to influence the work reported in this paper.

☐The authors declare the following financial interests/personal relationships which may be considered as potential competing interests: